Supplementary information

Tailoring the Cavities of Hydrogen-bonded Amphidynamic Crystals using Weak Contacts: Towards Faster Molecular Machines

Armando Navarro-Huerta[‡], Marcus J. Jellen[†], Jessica Arcudia[§], Simon J. Teat[#], Rubén A. Toscano[‡], Gabriel Merino[*§] and Braulio Rodríguez-Molina[*,‡]

[‡]*Instituto de Química, Universidad Nacional Autónoma de México, Circuito Exterior, Ciudad Universitaria, 04510, Ciudad de México, México.*

[†]*Department of Chemistry and Biochemistry, University of California, Los Angeles, California 90095, United States.*

[#]*Advanced Light Source, Lawrence Berkeley National Laboratory, Berkeley, California 94720-8229, United States.*

[§]*Departamento de Física Aplicada, Centro de Investigación y de Estudios Avanzados, Unidad Mérida. Km 6 Antigua Carretera a Progreso. Apdo. Postal 73, Cordemex, Mérida, 97310, Yucatán, México.*

*gmerino@cinvestav.mx

*brodriguez@iquimica.unam.mx

Contents

Materials and methods

Reagents and solvents were purchased from company Sigma-Aldrich® and were used without further purification. Reactions were monitored through TLC using silica gel plates 60 F_{254} purchased from Merck®. Spots were detected either by UV-light absorption or by using Seebach's TLC stain. Reactions were carried out in inert atmosphere using nitrogen (N_2). Solution ^{1}H and ^{13}C experiments were recorded at room temperature using Bruker Avance III 400 with BBO 400S1 probe or with Jeol Eclipse 300. The spectroscopic data is referenced to $CDCl_3$ (^{1}H: δ = 7.26 ppm, s; ^{13}C: δ = 77.0 ppm) or DMSO-d_6 (^{1}H, δ = 2.5 ppm, q; ^{13}C: δ = 39.52 ppm). High-Resolution Mass Spectrometry was obtained in a Jeol JMS-AccuTOF JMS-T100LC spectrometer, ionization mode: Direct Analysis in Real Time (DART). FTIR spectra experiments were recorded with Bruker ATR equipped with a diamond tip in the spectral window from 4000 to 500 cm^{-1}. Uncorrected melting points were determined in a Fisher-Johns melting point apparatus, unless otherwise noted.

Synthesis of 1,4-diazabiciclo[2.2.2]octane-d_{10} (DABCO-d_{10}) was followed as described in a procedure already reported.[S1] M.P. 112-114 °C, ***MS*** (DART) m/z: $[M+H]^+$: 121.15477 (D_8, 11.8%), 122.15622 (D_9, 35.2%), 123.16125 (D_{10}, 74.9%), 124.16953 (D_{11}, 100%), 125.17496 (D_{12}, 87.6%), which account for 93% mean content of ^{2}H.

General procedure for the synthesis of carbazole-based stators via Suzuki coupling

Solid reagents were placed in a two-neck round-bottom flask with magnetic stirrer, connected to a reflux system, then sealed and degassed with N_2 for 20 minutes. Subsequently, solvents and solutions were poured using a syringe. In the reactions to obtain compounds **4** to **7** the system was heated to 85 °C with a heating mantle and left to react for the indicated time. The products were isolated using column chromatography with silica gel as stationary phase and hexanes to remove remaining starting materials, followed by a mixture of hexanes/ethyl acetate (97:3).

Compounds **4** to **6** were synthesized using the following quantities of reagents: 0.500 g of 3,6-diiodo-*9H*-carbazole (**8**) (1.0 eq, 1.19 mmol), 0.564 g of the corresponding difluorophenylboronic acid (3.0 eq, 3.58 mmol), 0.042 g of $Pd(PPh_3)_2Cl_2$ (0.05 eq, 0.06 mmol), 8 mL of toluene, 0.8 mL of ethanol and 1 mL of K_2CO_3 (2 mol L^{-1}).

3,6-bis(2,4-difluorophenyl)-*9H*-carbazole (4)

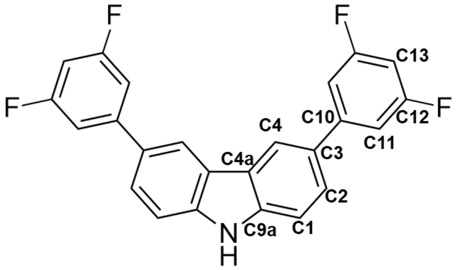

Reaction between 3,6-diiodo-*9H*-carbazole (**8**) and 3,5-difluorophenylboronic acid. Reaction time of 12 hours. The product was recovered as a white, granular solid (0.260 g, **yield 56%**, **m.p.** 165-167). **^{1}H NMR** (400 MHz, $CDCl_3$) δ: 8.29 (s, 2H, H4), 8.19 (s, 1H, H9), 7.65 (dd, 2H, *J* = 8.5, 1.8 Hz, H2), 7.51 (d, 2H, *J* = 8.4 Hz, H1), 7.23 (d, 4H, *J* = 8.9, H11), 6.78 (tt, 2H, *J* = 8.9, 2.3 Hz, H13). **^{13}C NMR** (100 MHz, $CDCl_3$) δ: 163.6 (C12, dd, *J* = 246.5, 13.6 Hz), 145.3 (C3), 140.1 (C9a), 131.2 (C10), 125.7 (C2), 124.0 (C4a), 119.1 (C4), 111.4 (C1), 110.0 (C11, d, *J* = 25.2 Hz), 101.9 (C13, t, *J* = 25.5 Hz). **FTIR** (ATR, cm^{-1}) ν: 3470, 1623, 1591, 1468, 1288, 1243, 1194, 1110, 986, 848, 803, 616. **HRMS** (DART) m/z: $[C_{24}H_{14}F_4N]^+$, calculated 392.10624, found 392.10690, difference (ppm): 1.70.

3,6-bis(2,5-difluorophenyl)-*9H*-carbazole (5)

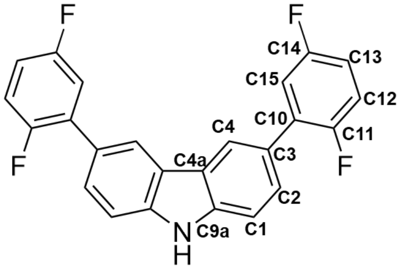

Reaction between 3,6-diiodo-*9H*-carbazole (**8**) and 2,5-difluorophenylboronic acid. Reaction time of 14 hours. The product was recovered as a white, fine solid (0.223 g, **yield 48%**, **m.p.** 151-153 °C). **^{1}H NMR** (400 MHz, $CDCl_3$) δ: 8.27 (s, 2H, H4), 8.15 (s, 1H, H9), 7.63 (d, 2H, *J* = 8.4 Hz, H2), 7.49 (d, 2H, *J* = 8.4 Hz, H1), 7.29 – 7.24 (m, 2H, H15), 7.15 (td, *J* = 9.5, 4.5 Hz, 2H, H12), 7.03 – 6.97 (m, 2H, H13). **^{13}C NMR** (100 MHz, $CDCl_3$) δ: 159.0 (C11, d, *J* = 240.7 Hz), 156.0 (C14, d, *J* = 243.6 Hz), 139.7 (C9a), 131.1 (C10, dd, *J* = 24.4, 7.7 Hz), 127.3 (C2), 126.6 (C3), 123.7 (C4a), 121.1 (C4), 117.4 (C12), 117.1 (C15), 114.6 (C13, dd, *J* = 24.0, 8.4 Hz), 110.9 (C1). **FTIR** (ATR, cm^{-1}) ν: 3428, 1607, 1490, 1240, 1177, 1101, 875, 802, 761, 701, 617. **HRMS** (DART) m/z: $[C_{24}H_{14}F_4N]^+$, calculated 392.10624, found 392.10699, difference (ppm): 1.92.

3,6-bis(2,3-difluorophenyl)-*9H*-carbazole (6)

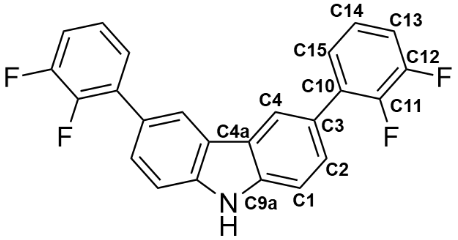

Reaction between 3,6-diiodo-*9H*-carbazole (**8**) and 2,3-difluorophenylboronic acid. Reaction time of 10 hours. The product was recovered as a white, fine solid (0.242 g, **yield 52%**, **m.p.** 144-146 °C). **^{1}H NMR** (400 MHz, CDCl$_3$) δ: 8.27 (s, 2H, H4), 8.17 (s, 1H, H9), 7.64 (d, 2H, J = 8.4 Hz, H2), 7.50 (d, 2H, J = 8.4 Hz, H1), 7.33 – 7.30 (m, 2H, H15), 7.18 – 7.10 (m, 4H, H13, H14). **^{13}C NMR** (100 MHz, CDCl$_3$) δ: 151.9 (C12, dd, J = 237.3, 12.9 Hz), 148.2 (C11, dd, J = 248.2, 12.7 Hz), 139.7 (C9a), 132.1 (C10, d, J = 10.2 Hz), 127.4 (C2), 126.5 (C3), 125.8 (C15), 124.2 (C14), 123.7 (C4a), 121.1 (C4), 115.5 (C13, d, J = 17.4 Hz), 110.9 (C1). **FTIR** (ATR, cm^{-1}) ν: 3478, 2923, 1609, 1477, 1260, 897, 770. **HRMS** (DART) m/z: [C$_{24}$H$_{14}$F$_4$N]$^+$, calculated 392.10624, found 392.10818, difference (ppm): 4.95.

3,6-diphenyl-9H-carbazole (7)

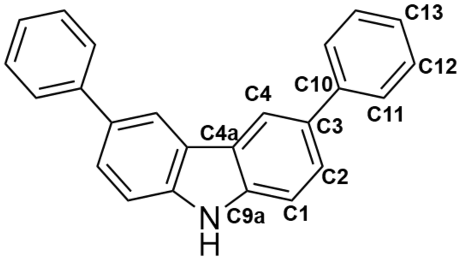

Reaction time of 24 hours. Quantities: 0.500 g of 3,6-diiodo-9H-carbazole **(8)** (1.0 eq, 1.19 mmol), 0.436 g of phenylboronic acid (3.0 eq, 3.58 mmol), 0.042 g of Pd(PPh$_3$)$_2$Cl$_2$ (0.05 eq, 0.06 mmol), 8 mL of toluene, 0.8 mL of ethanol and 1 mL of K$_2$CO$_3$ (2 mol L^{-1}). The product was recovered as a white solid (0.192 g, **yield 50%**, **m.p.** 204-205 °C). **^{1}H NMR** (400 MHz, CDCl$_3$) δ: 8.35 (s, 2H, H4), 8.03 (s, 1H, H9), 7.75 (d, J = 7.9 Hz, 4H, H11), 7.71 (d, J = 8.3 Hz, 2H, H2), 7.52 (t, J = 8.0 Hz, 4H, H12), 7.47 (d, J = 8.6 Hz, 2H, H1), 7.38 (t, J = 7.4 Hz, 2H, H13). **^{13}C NMR** (100 MHz, CDCl$_3$) δ: 142.1 (C9a), 139.5 (C3), 133.3 (C10), 128.9 (C12), 127.4 (C11), 126.7 (C13), 125.8 (C2), 124.1 (C4a), 119.0 (C4), 111.0 (C1). **FTIR** (ATR, cm^{-1}) ν: 3418, 3032, 2924, 2853, 1601, 1475, 1283, 1238, 822, 761, 697. **HRMS** (DART) m/z: [C$_{24}$H$_{18}$N]$^+$, calculated 320.14392, found 320.14463, difference (ppm): 2.20.

3,6-diiodo-*9H*-carbazole (8)

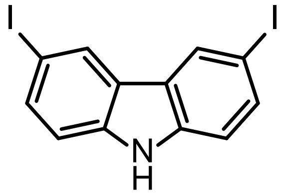

In a two-neck round-bottom flask attached to a condenser were placed the next quantities of reagents: 0.500 g (1.0 eq., 2.99 mmol) of carbazole, 0.650 g of KIO_3 (1.0 eq., 3.04 eq) and 0.650 g of KI (1.3 eq, 3.91 mmol). The flask was sealed and degassed with N_2 for 15 minutes, then 10 mL of glacial acetic acid were added. The mixture was heated to 85 °C and left to react for 50 minutes. Afterwards, the residue was poured into an ice-bath with Na_2SO_3 and stirred for 20 minutes. The solid formed was vacuum filtered and recrystallized from ethanol to afford a fine, gray, crystalline solid (0.952 g, **yield 76%**, **m.p.** 209-211 °C). **^{1}H NMR** (300 MHz, DMSO-d_6) δ: 11.56 (s, 1H), 8.57 (s, 2H), 7.66 (dd, 2H, *J* = 8.5, 1.7 Hz), 7.35 (d, 2H, *J* = 8.5 Hz) . **^{13}C NMR** (75 MHz, DMSO-d_6) δ: 138.8, 134.1, 129.2, 123.9, 113.6, 81.9. **FTIR** (ATR, cm^{-1}) ν: 3410, 1867, 1736, 1560, 818, 418. **HRMS** (DART) m/z: $[C_{12}H_8NI_2]^+$, calculated 419.87461, found 419.87560, difference (ppm): 2.36.

General procedure for synthesis of single crystals of cocrystals 1-3I and 7s

In a 6 mL capped vial were placed two equivalents of compounds **4** to **7** by one equivalent of DABCO. Afterwards, to the solution was added 3 mL of a (95:5 v/v%) hexane:ethyl acetate solvent mixture, the vial was sealed and heated for 20 minutes or until all the solids had solubilized. The vial was left to cool down to room temperature with a loose cap to allow the solvent to slowly evaporate. The vial is placed in fridge for a week to allow larger crystals to form.

Table S1. Melting points of cocrystals herein described

Cocrystal	Melting point (°C)
1	157-159
2	156-158
3 (form I)	149-150
7s	154-156

General procedure for obtaining of cocrystals 1 to 3I in bulk via mechanochemical synthesis

For cocrystals **1-3I**, two equivalents of the corresponding carbazole moiety were placed in an agate mortar along with one equivalent of DABCO (or DABCO-d_{10} for deuterated rotors). Then, 4 drops of Na/benzophenone dried THF are poured into the mixture. The resulting paste was manually grinded with the agate pestle for 5 minutes, which produced an off-white pulverized solid.

Optical Microscopy

Optical microscopy images were acquired using an Olympus BX43 microscope with a QImaging MicroPublisher camera (5.0 MP RTV), using freshly grown single crystals of each rotor.

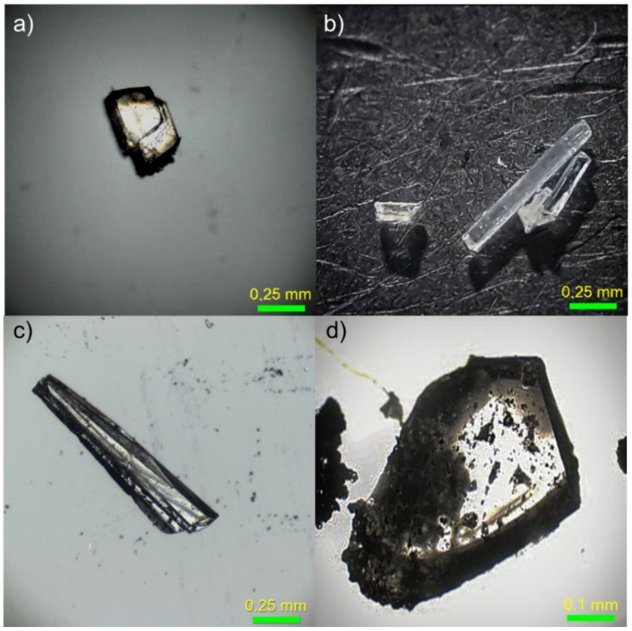

Figure S1. Optical microscopy pictures of freshly grown single crystals described in this work. In this order a) **1**, b) **2**, c) **3I** and d) **7s**.

Solution ^{1}H and ^{13}C NMR characterization of compounds

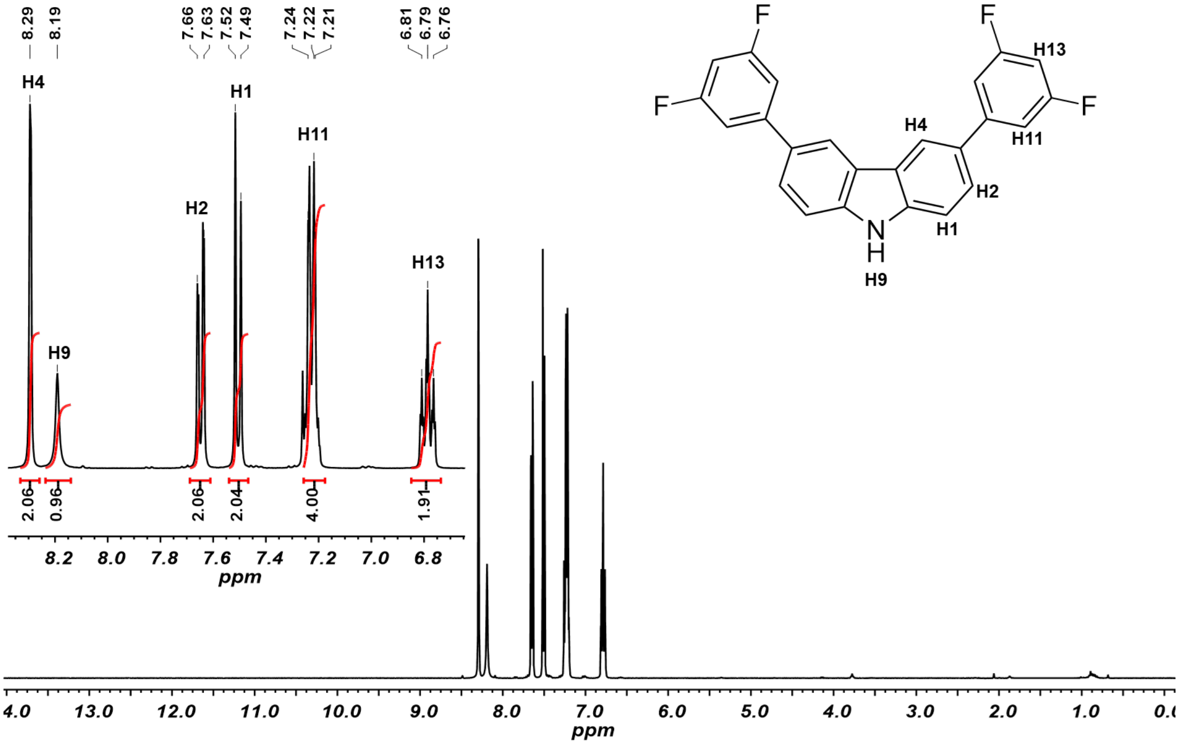

Figure S2. ^{1}H solution NMR spectra of **4** (CDCl$_3$, 400 MHz)

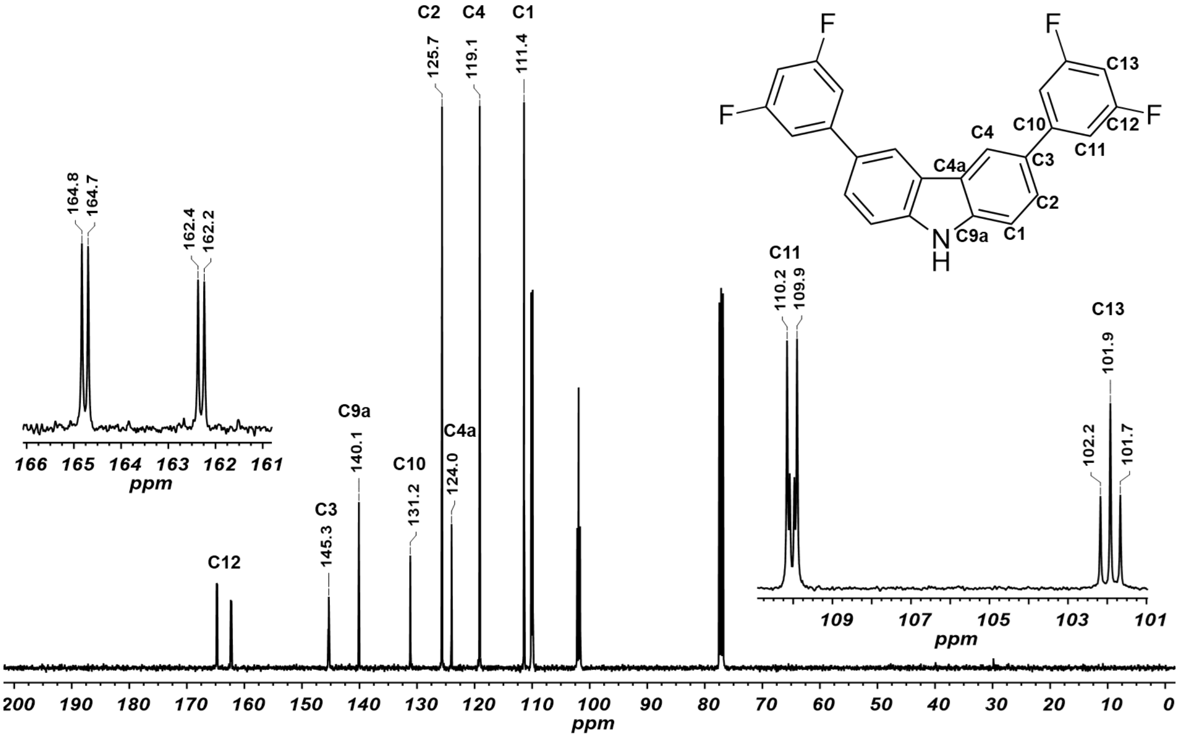

Figure S3. ^{13}C solution NMR spectra of **4** (CDCl$_3$, 100 MHz)

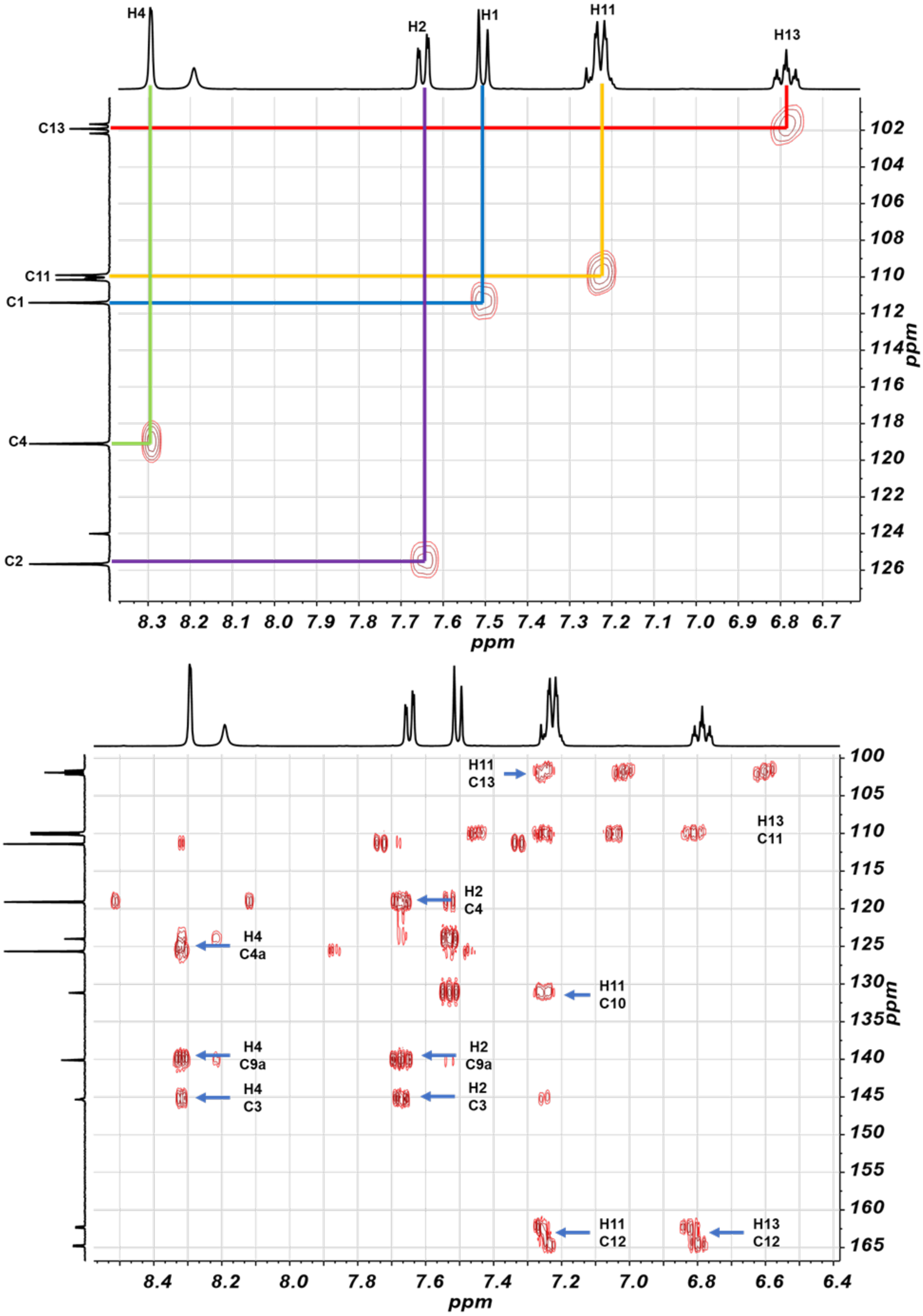

Figure S4. 2D NMR spectra of compound **4** (HSQC, up and HMBC, down).

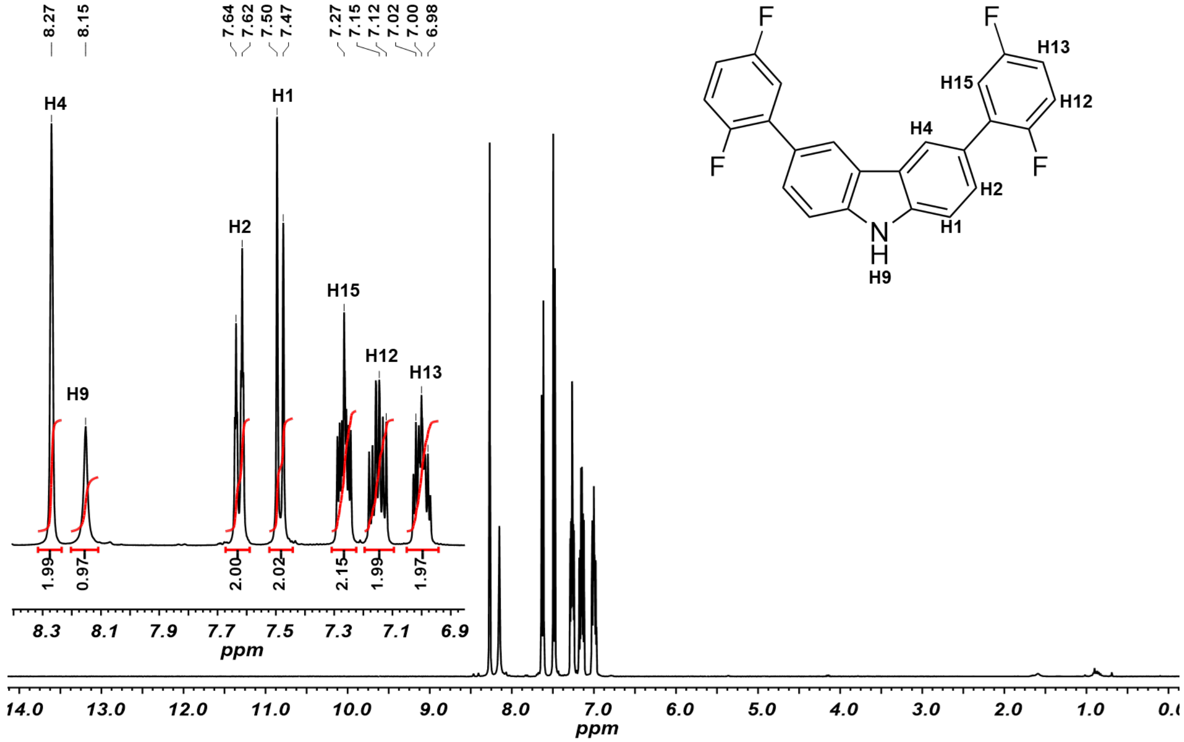

Figure S5. ^{1}H solution NMR spectra of **5** ($CDCl_3$, 400 MHz)

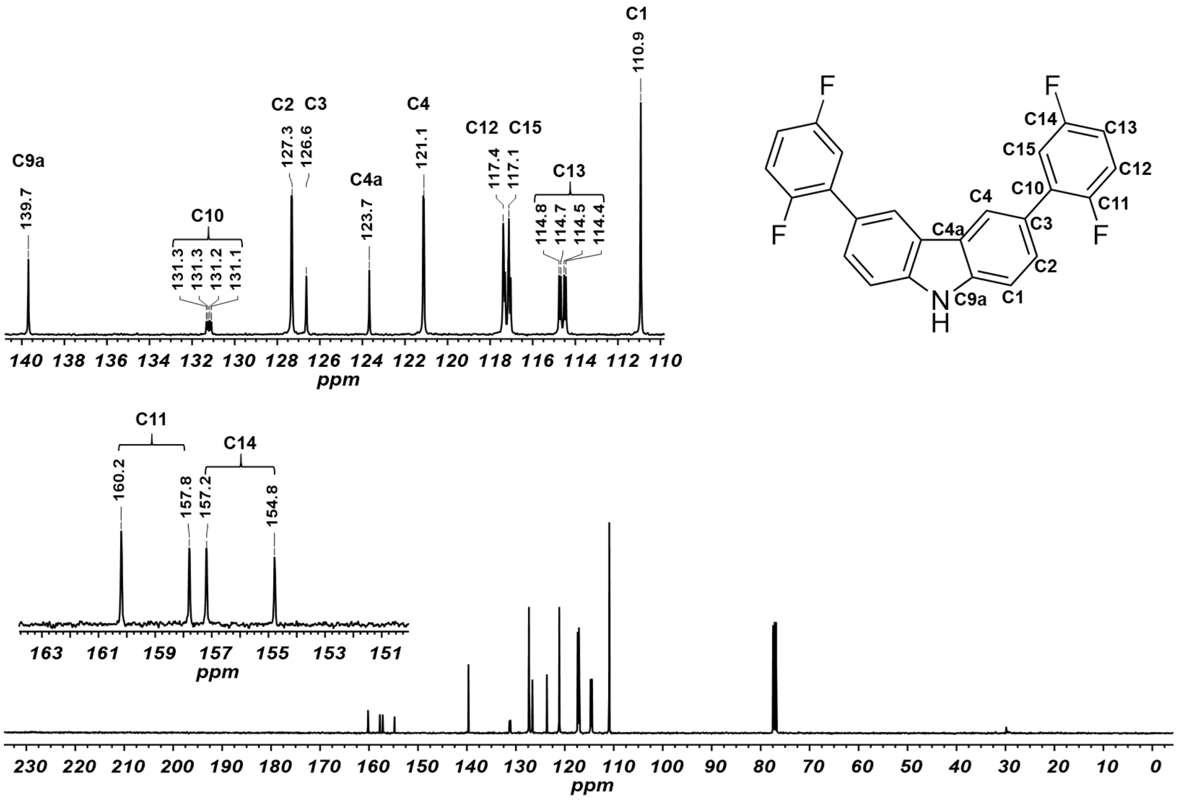

Figure S6. ^{13}C solution NMR spectra of **5** ($CDCl_3$, 100 MHz)

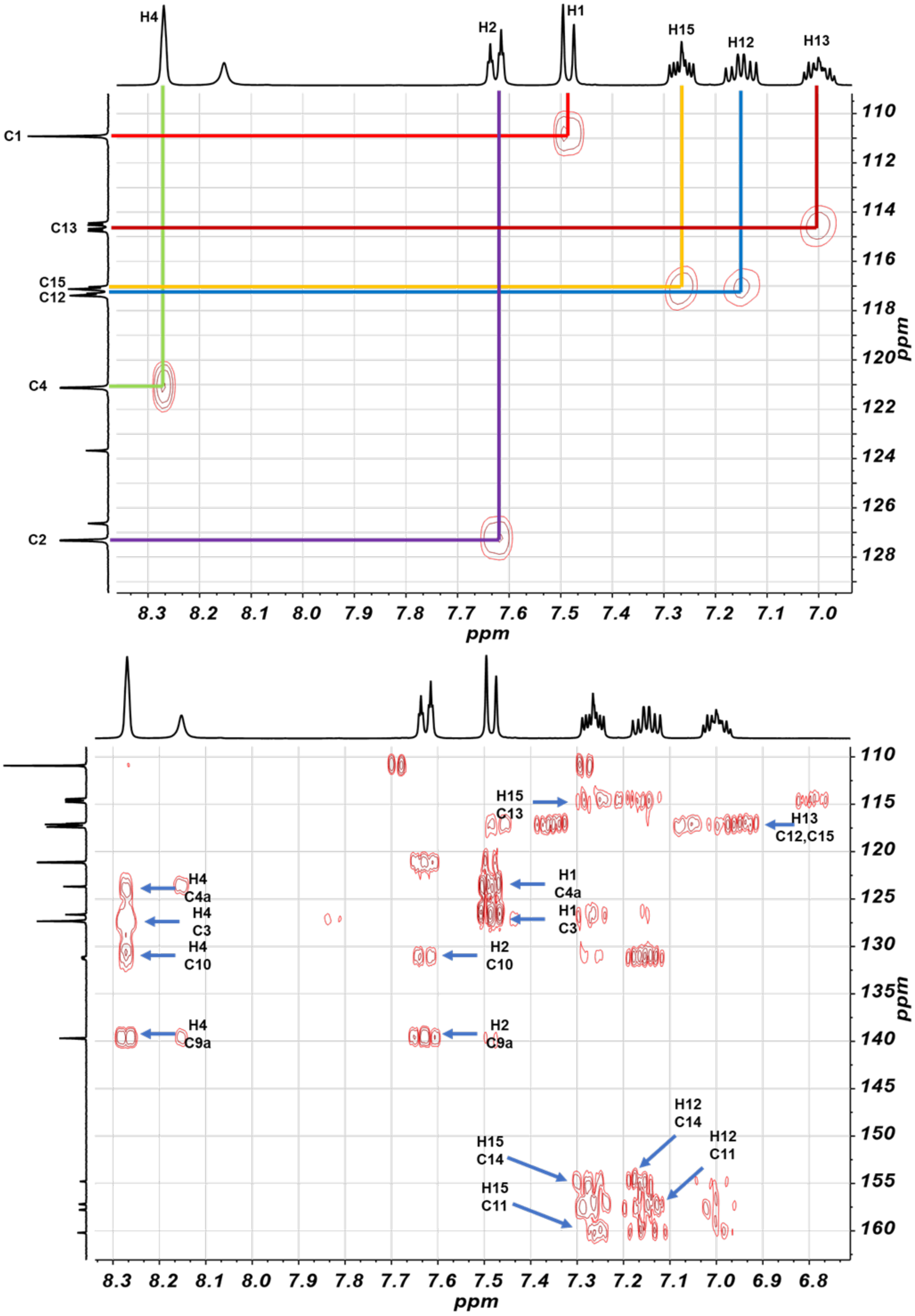

Figure S7. 2D NMR spectra of compound **5** (HSQC, up and HMBC, down).

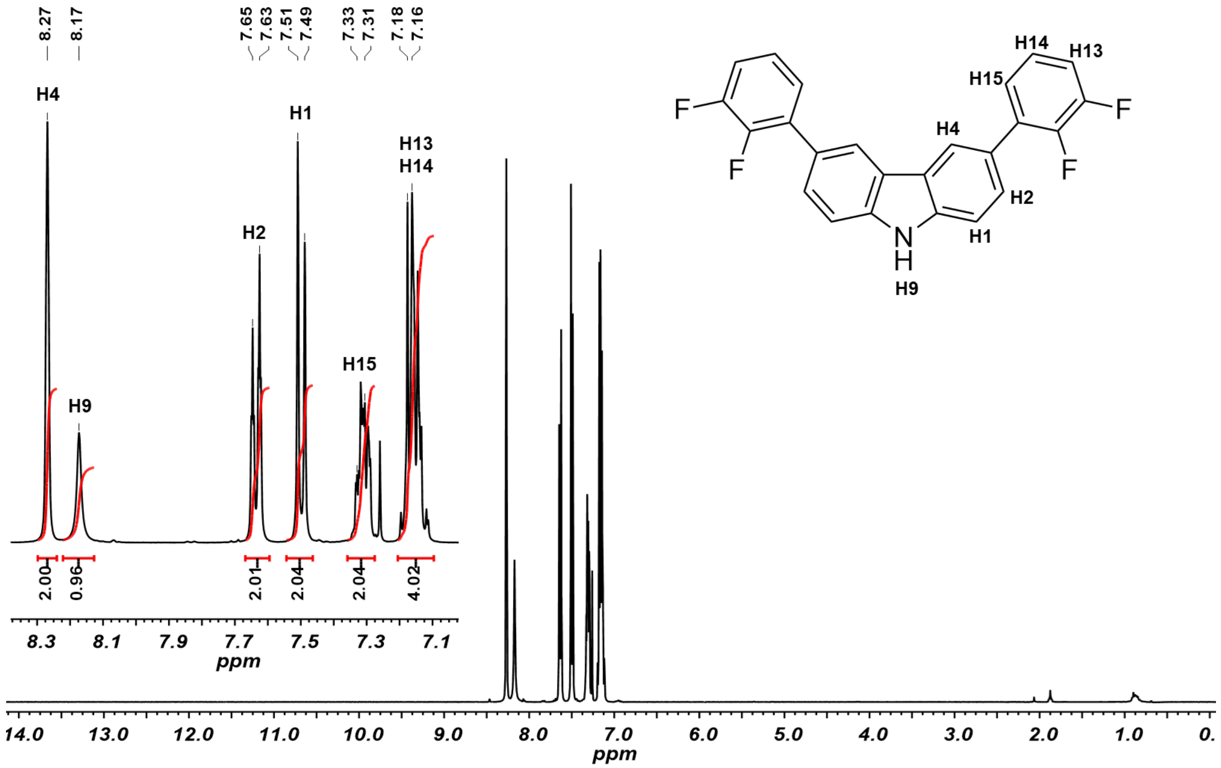

Figure S8. ^{1}H solution NMR spectra of **6** ($CDCl_3$, 400 MHz)

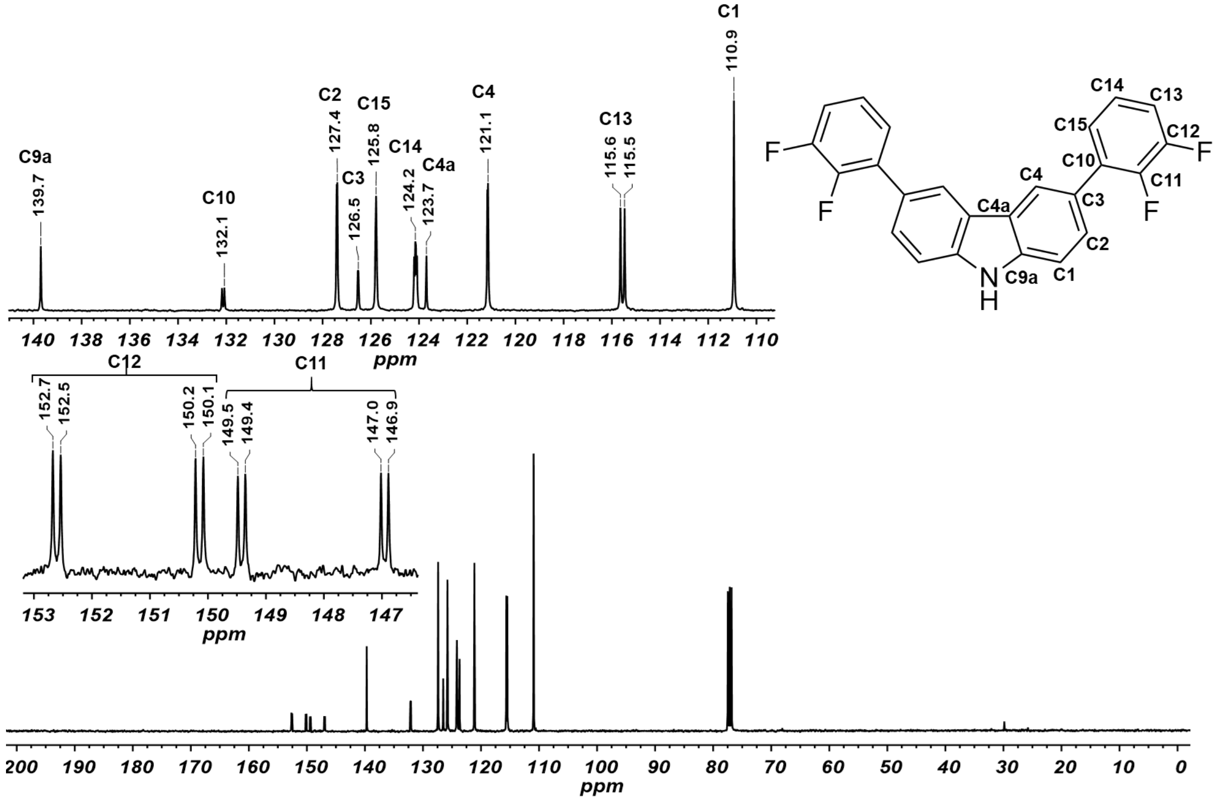

Figure S9. ^{13}C solution NMR spectra of **6** ($CDCl_3$, 100 MHz)

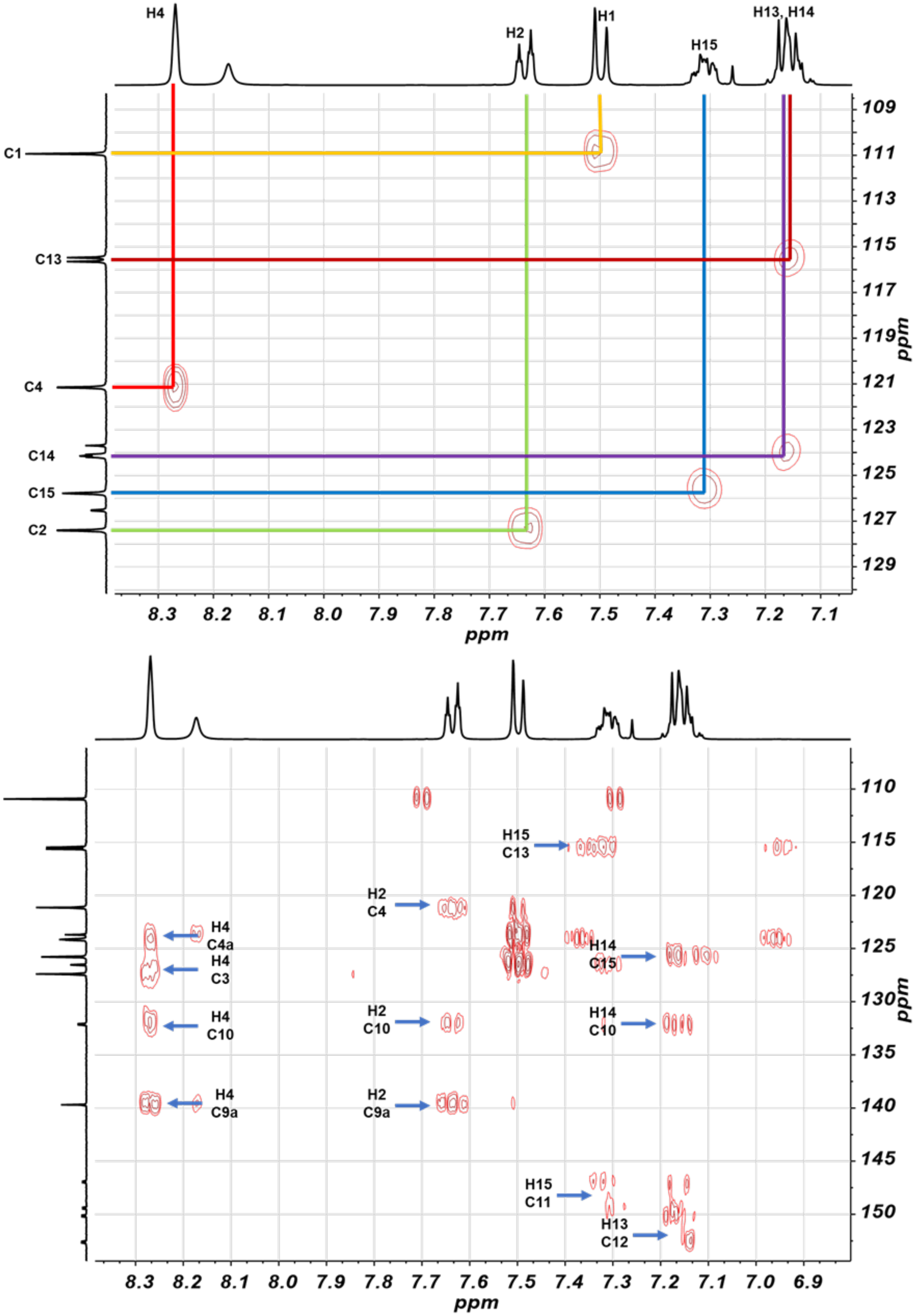

Figure S10. 2D NMR spectra of compound **6** (HSQC, up and HMBC, down).

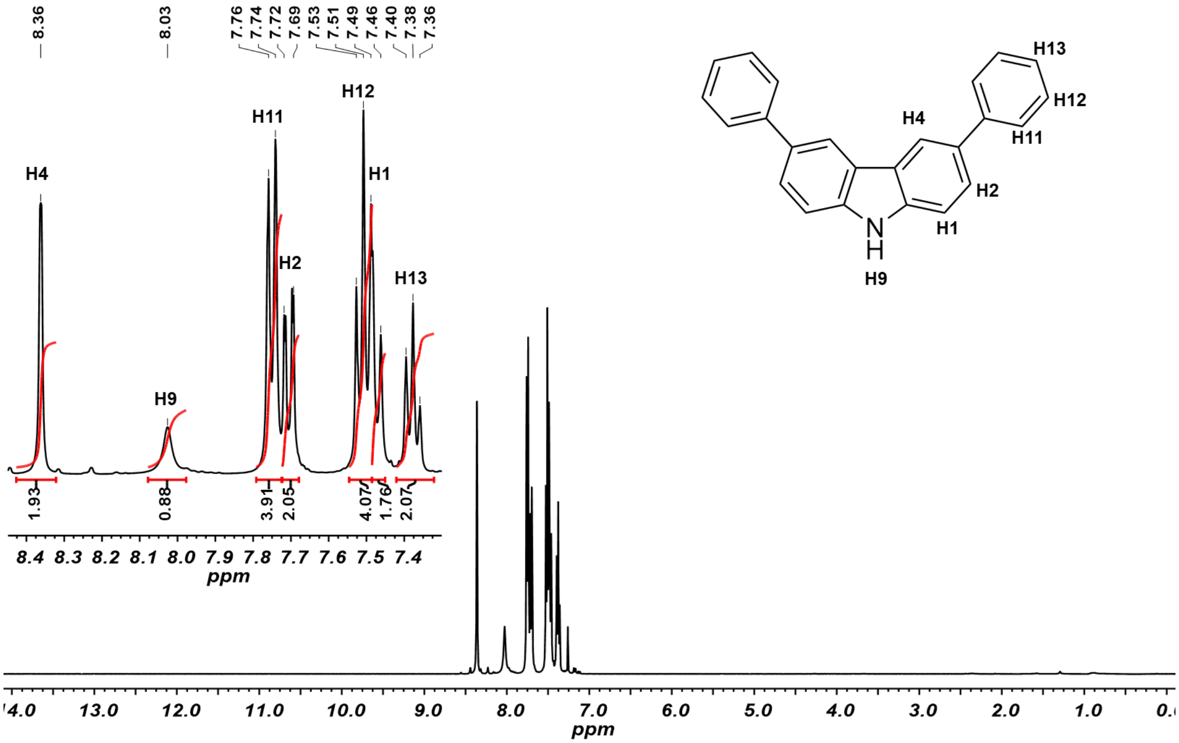

Figure S11. ^{1}H solution NMR spectra of **7** ($CDCl_3$, 400 MHz)

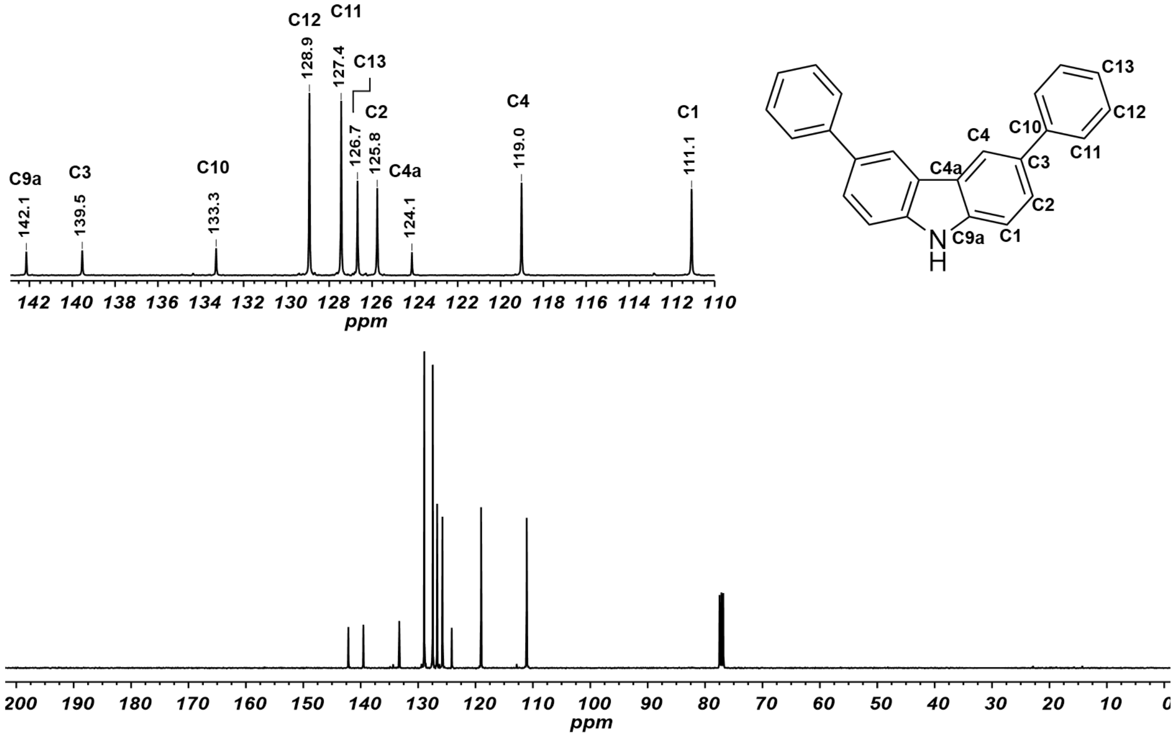

Figure S12. ^{13}C solution NMR spectra of **7** ($CDCl_3$, 100 MHz)

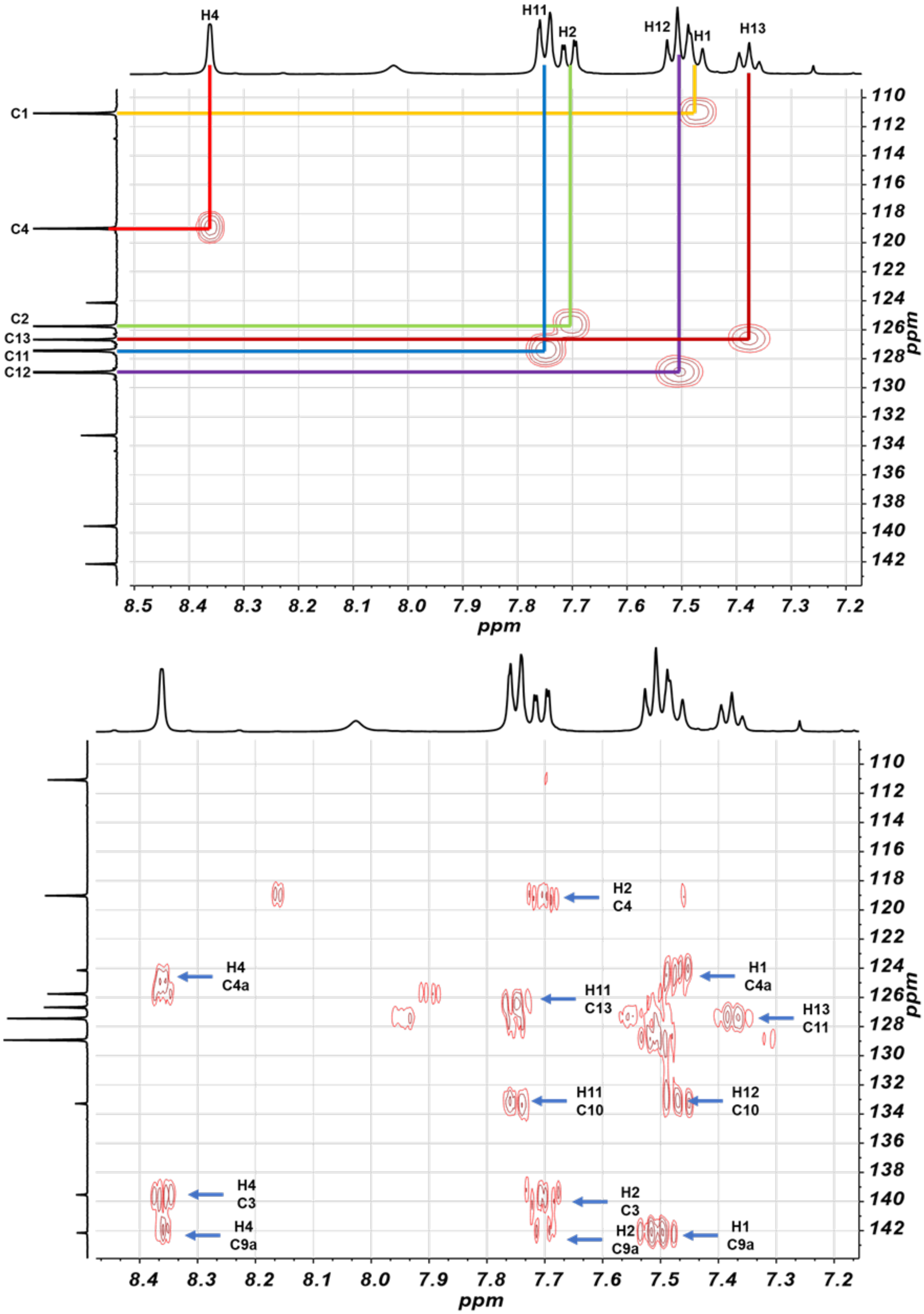

Figure S13. 2D NMR spectra of compound **7** (HSQC, up and HMBC, down).

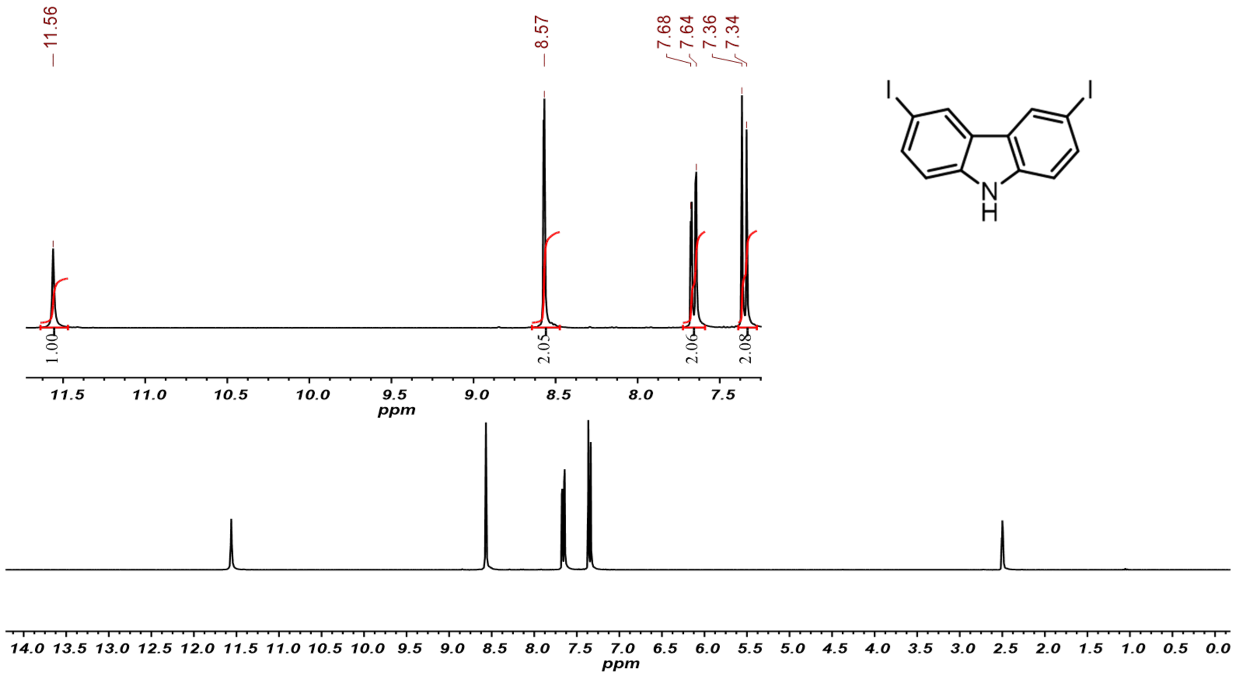

Figure S14. ^{1}H solution NMR spectra of **8** (DMSO-d_6, 300 MHz)

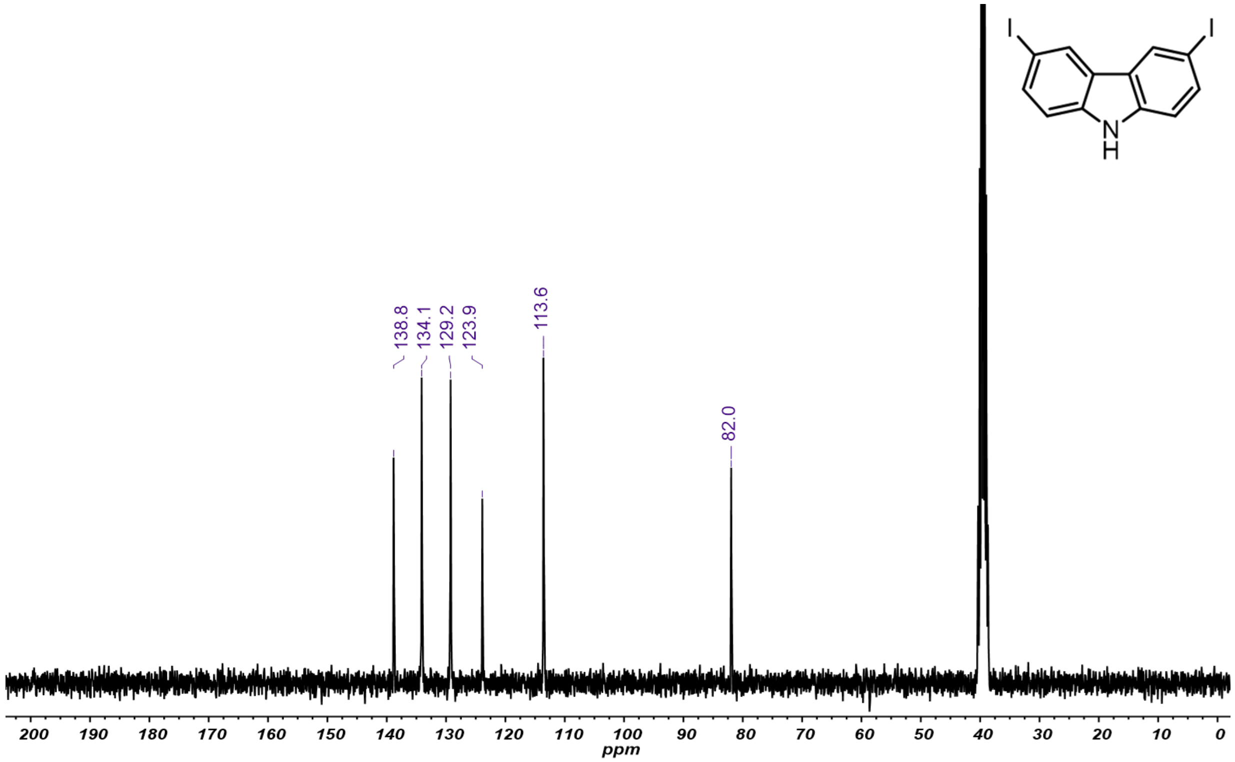

Figure S15. ^{13}C solution NMR spectra of **8** (DMSO-d_6, 75 MHz)

^{1}H NMR spectra. Recognition experiments

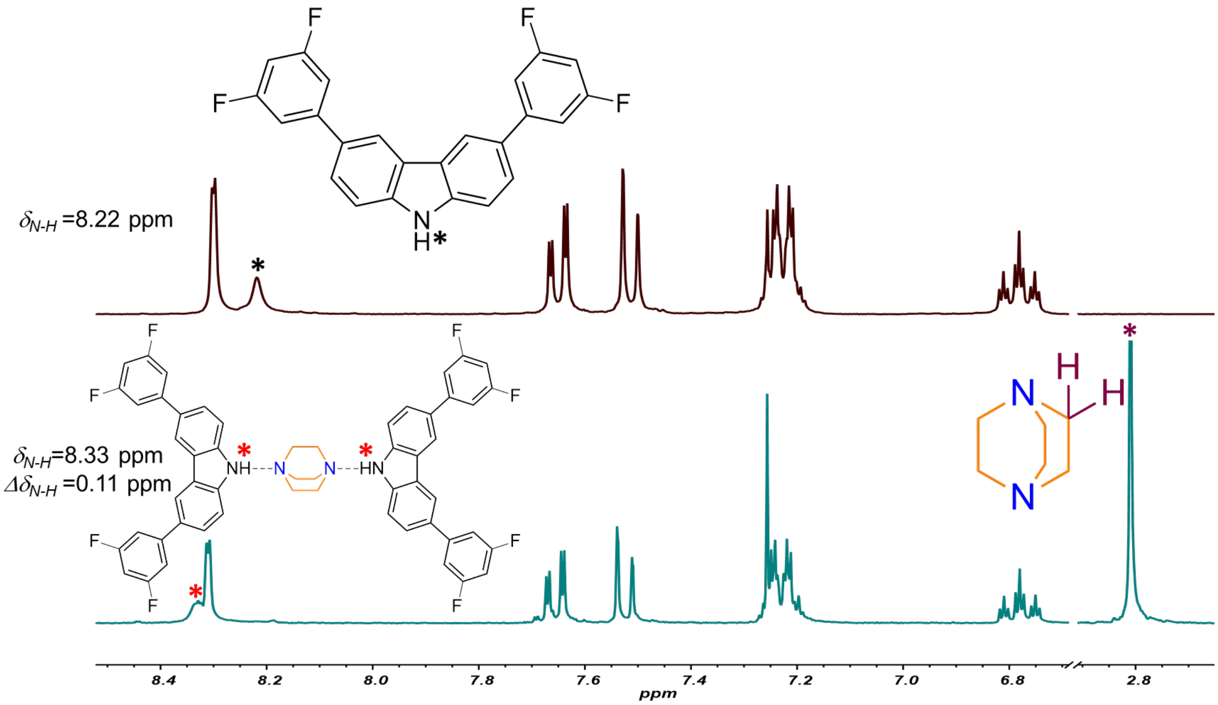

Figure S16. Stacked ^{1}H solution NMR spectra ($CDCl_3$, 300 MHz, both) of pure **4** (top) and mixture 2:1 **4+DABCO** (bottom)

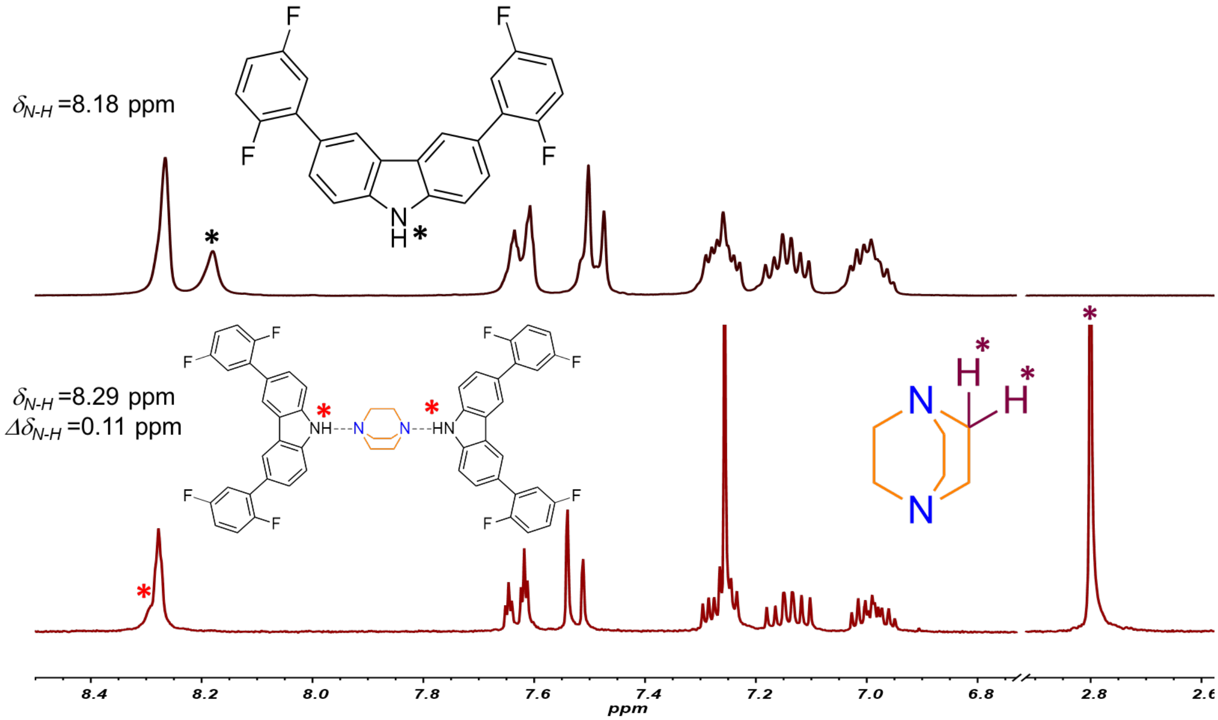

Figure S17. Stacked ^{1}H solution NMR spectra ($CDCl_3$, 300 MHz, both) of pure **5** (top) and mixture 2:1 **5+DABCO** (bottom)

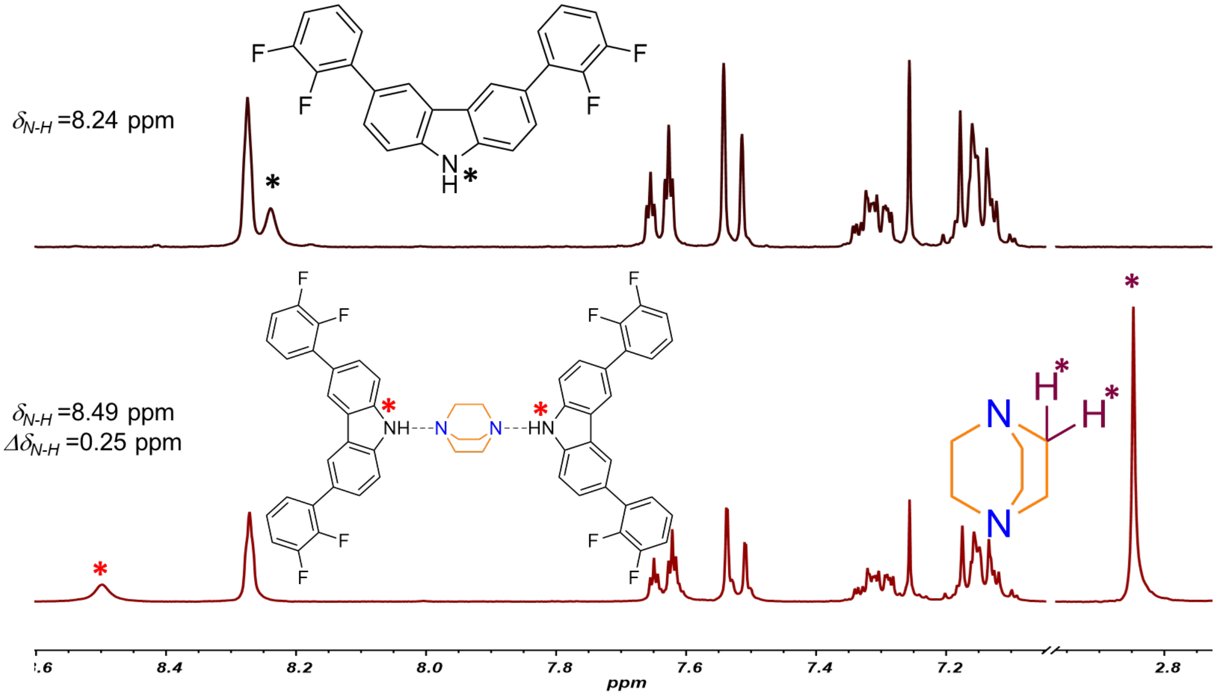

Figure S18. Stacked ^{1}H solution NMR spectra ($CDCl_3$, 300 MHz, both) of pure **6** (top) and mixture 2:1 **6+DABCO** (bottom)

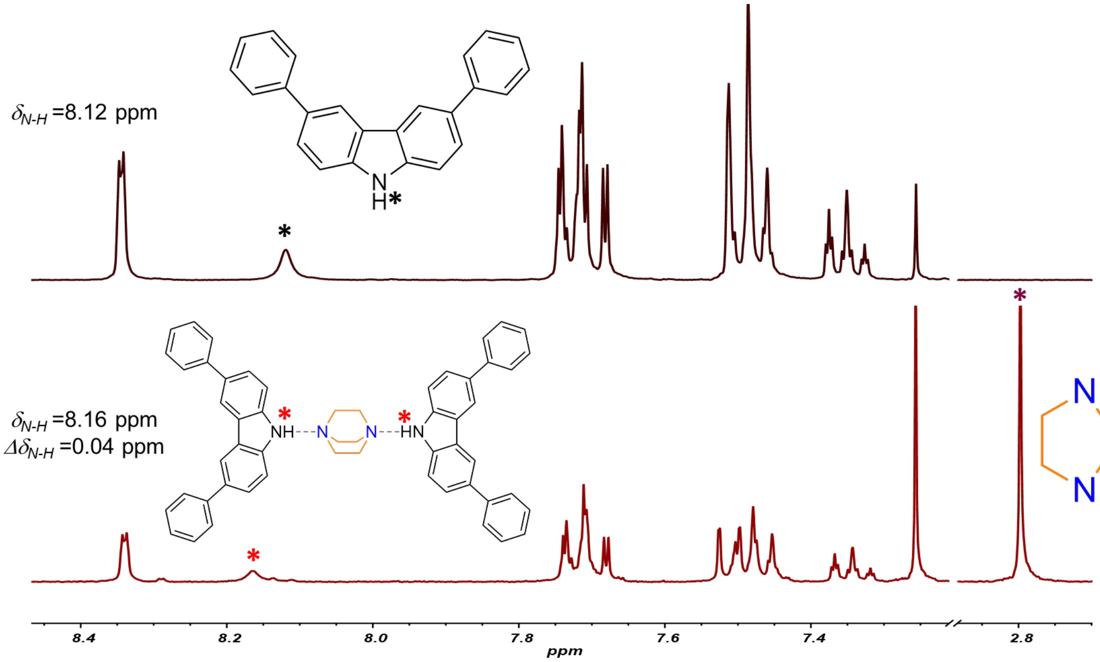

Figure S19. Stacked ^{1}H solution NMR spectra ($CDCl_3$, 300 MHz, both) of pure **7** (top) and mixture 2:1 of **7**+**DABCO** (bottom)

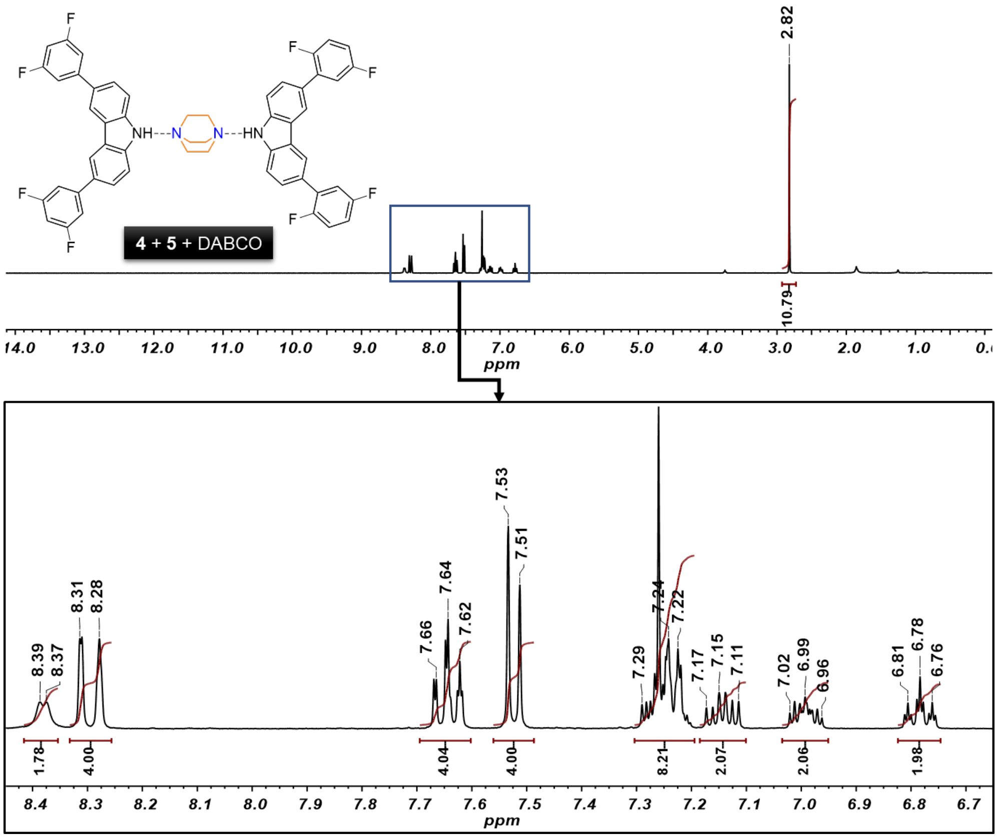

Figure S20. ^{1}H NMR solution spectra of mixture (1:1:1) **4+DABCO+5** (CDCl$_3$, 400 MHz)

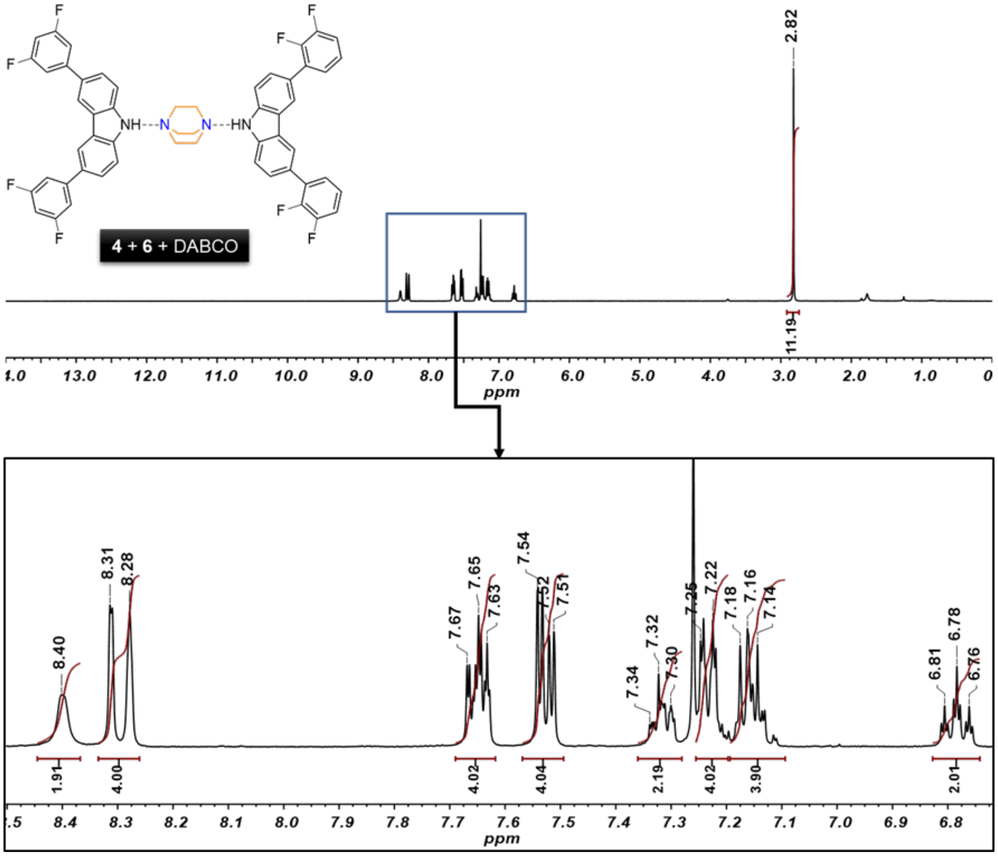

Figure S21. ^{1}H NMR solution spectra of mixture (1:1:1) **4+DABCO+6** (CDCl$_3$, 400 MHz)

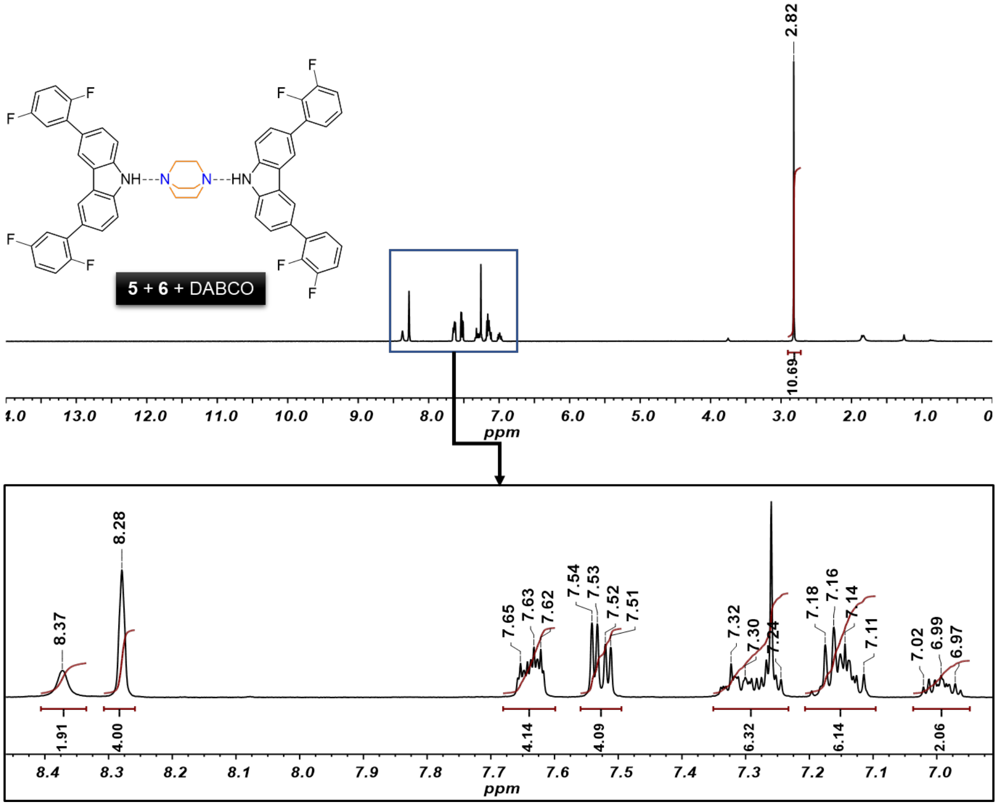

Figure S22. ^{1}H NMR solution spectra of mixture (1:1:1) **5+DABCO+6** ($CDCl_3$, 400 MHz)

Table S2. Chemical shifts of ^{1}H in solution NMR for the recognition experiments with DABCO

Compound	**4**	**5**	**6**	**7**
4	*8.33*			
5	*8.39, 8.37*	*8.29*		
6	*8.40*	*8.37*	*8.49*	
7	-	-	-	*8.33*

Crystallographic information tables and X-Ray diffraction studies

X-Ray diffraction data were obtained at variable temperature either from Bruker D8 diffractometer equipped with a PHOTON II CPAD detector with synchrotron radiation (λ=0.7288 Å) on beamline 12.2.1 at Advanced Light Source, or from Bruker Smart APEX II CCD[S2] with graphite monochromatic MoKα radiation (λ=0.71073 Å), as noted in the following tables. Cell refinement was carried out using SAINT V8.38A.[S3] Structure solution, final refinement and data output was carried out using SHELX-2014[S4] through direct methods. Non-hydrogen atoms were refined anisotropically and hydrogen atoms were placed in geometrically calculated positions using a riding model, with isotropic thermal parameters $U_{iso}(H) = 1.2U_{eq}(C)$. Crystal structures were generated with Mercury 4.3.1.[S5]

Powder X-Ray diffraction data were collected at room temperature in a Bruker D2 PHASER diffractometer, using CuKα radiation (λ=1.5406 Å), operating at 30 kV and 10 mA with a θ–θ configuration in a 2θ interval of 5-45°, step of 0.02°, time 0.250 s.

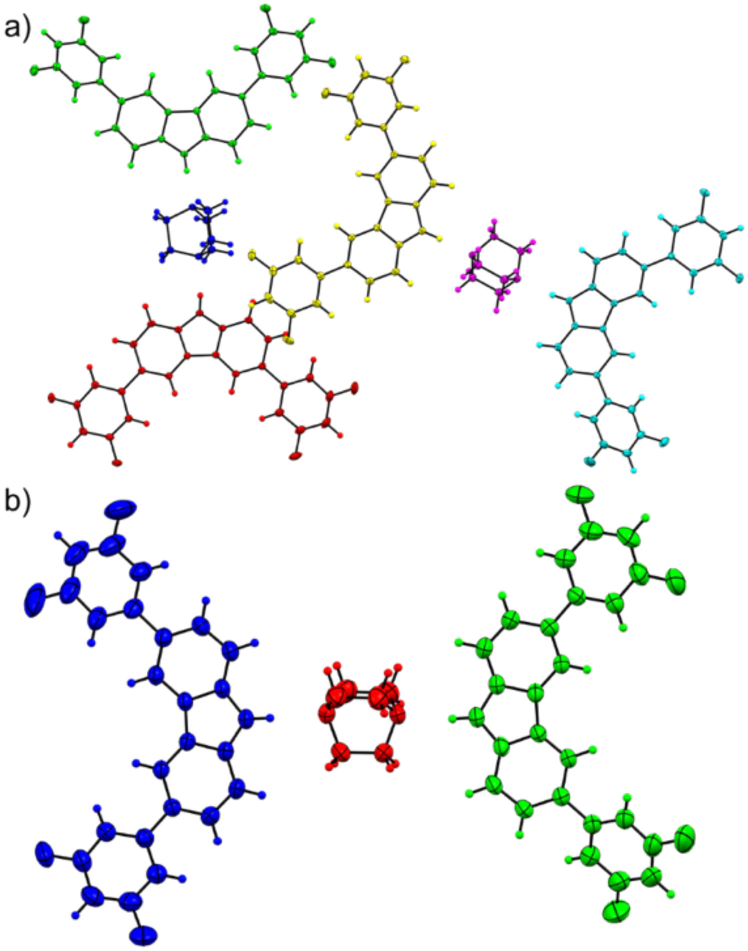

Figure S23. Asymmetric unit for cocrystal **1** at a) 100, 150 and 200 K (LT), and b) at 300 K (HT). Ellipsoids are drawn at 50% probability level. Colors used account for symmetry equivalent components.

Table S3. Crystallographic parameters for **1**

Formula	**$2(C_{24}H_{13}F_4N)\cdot C_6H_{12}N_2$**	**$2(C_{24}H_{13}F_4N)\cdot C_6H_{12}N_2$**	**$2(C_{24}H_{13}F_4N)\cdot C_6H_{12}N_2$**	**$2(C_{24}H_{13}F_4N)\cdot C_6H_{12}N_2$**[S6]	**$2(C_{24}H_{13}F_4N)\cdot C_6H_{12}N_2$**[S7]
Formula weight	894.88	894.88	894.88	894.88	894.88
Temperature (K)	100(2)	150(2)	200(2)	250(2)	300(2)
System	monoclinic	monoclinic	monoclinic	monoclinic	monoclinic
Space Group	$P2_1$	$P2_1$	$P2_1$	$P2_1$	*C*c
a (Å)	14.0179(5)	14.0331(4)	14.0444(4)	14.0592(6)	13.9524(6)
b (Å)	13.6325(5)	13.6998(4)	13.7744(4)	13.8649(6)	14.0942(5)
c (Å)	22.7651(7)	22.8049(7)	22.8418(7)	22.8854(9)	22.7794(8)
α (°)	90	90	90	90	90
β (°)	107.5360(10)	107.5550(10)	107.5900(10)	107.6288(14)	106.4326(15)
γ (°)	90	90	90	90	90
ρ (g/cm^3)	1.433	1.422	1.411	1.398	1.383
V (Å^3)	4148.2(2)	4180.1(2)	4212.2(2)	4251.5(3)	4296.5(3)
Z	4	4	4	4	4
Absoption coefficient (mm^{-1})	0.114	0.114	0.113	0.112	0.110
F(000)	1848	1848	1848	1848	1848
Crystal size (mm)	0.100 x 0.090 x 0.030	0.100 x 0.090 x 0.030	0.100 x 0.090 x 0.030	0.100 x 0.090 x 0.030	0.100 x 0.090 x 0.030
Radiation [λ (Å)]	Synchrotron (0.7288)	Synchrotron (0.7288)	Synchrotron (0.7288)	Synchrotron (0.7288)	Synchrotron (0.7288)
Collected reflections	148821	145863	144945	*	20394
Independent reflections	23303	22549	22733	*	5794
Data/rest/param	23303/1/1201	22549/1/1201	22733/1/1201	*	5794/2/602
GooF	1.029	1.037	1.025	*	1.047
Final R indexes [$I_0>2\sigma(I_0)$]	R_1=0.0337 wR_2=0.0884	R_1=0.0355 wR_2=0.0945	R_1=0.0412 wR_2=0.1098	*	R_1=0.0372 wR_2=0.0936
Final R indexes [all data]	R_1=0.0348 wR_2=0.0896	R_1=0.0372 wR_2=0.0965	R_1=0.0439 wR_2=0.1134	*	R_1=0.0471 wR_2=0.0993
Largest diff. peak/hole (eA^{-3})	0.317/-0.299	0.332/-0.237	0.341/-0.309	*	0.140/-0.165
CCDC number	2022170	2022171	2022172	*	2022173

Table S4. Hydrogen bond parameters in the two crystal phases of the supramolecular rotor **1**

100 K ($P2_1$)		**300 K (Cc)**	
Distance D-A (Å)	Angle N-H···N (°)	Distance D-A (Å)	Angle N-H···N (°)
2.840(2)	177(2)	2.884(3)	164(4)
2.876(2)	176(2)		
2.826(2)	175(2)	2.875(3)	166(4)
2.847(2)	174(2)		

Table S5. Crystallographic parameters for **2**

Formula	**$2(C_{24}H_{13}F_4N)\cdot C_6H_{12}N_2$**	**$2(C_{24}H_{13}F_4N)\cdot C_6H_{12}N_2$**	**$2(C_{24}H_{13}F_4N)\cdot C_6H_{12}N_2$**	**$2(C_{24}H_{13}F_4N)\cdot C_6H_{12}N_2$**	**$2(C_{24}H_{13}F_4N)\cdot C_6H_{12}N_2$**
Formula weight	894.88	894.88	894.88	894.88	894.88
Temperature (K)	100(2)	150(2)	200(2)	250(2)	302(2)
System	monoclinic	monoclinic	monoclinic	monoclinic	monoclinic
Space Group	$P2_1/n$	$P2_1/n$	$P2_1/n$	$P2_1/n$	$P2_1/n$
a (Å)	6.6570(3)	6.6613(3)	6.6696(2)	6.6803(2)	6.6761(5)
b (Å)	14.8520(6)	14.8875(6)	14.9431(5)	15.0128(5)	15.0587(11)
c (Å)	21.2537(8)	21.2797(8)	21.3309(7)	21.3972(7)	21.4293(14)
α (°)	90	90	90	90	90
β (°)	95.7210(10)	95.554(2)	95.362(2)	95.1430(10)	94.9412(17)
γ (°)	90	90	90	90	90
ρ (g/cm^3)	1.420	1.415	1.404	1.391	1.385
V (Å^3)	2090.88(15)	2100.40(15)	2116.63(12)	2137.29(12)	2146.4(3)
Z	2	2	2	2	2
Absorption coefficient (mm^{-1})	0.113	0.113	0.112	0.111	0.106
F(000)	922	924	924	924	924
Crystal size (mm)	0.340 x 0.120 x 0.100	0.340 x 0.120 x 0.100	0.340 x 0.120 x 0.100	0.340 x 0.120 x 0.100	0.413 x 0.368 x 0.298
Radiation [λ (Å)]	Synchrotron (0.7288)	Synchrotron (0.7288)	Synchrotron (0.7288)	Synchrotron (0.7288)	MoKα (0.71073)
Collected reflections	73120	60836	58731	60892	27821
Independent reflections	7264	6418	5448	5759	4923
Data/rest/param	7264/0/338	6418/0/338	5448/0/338	5759/0/338	4923/0/338
GooF	1.066	1.063	1.067	1.068	0.988
Final R indexes [$I_0>2\sigma(I_0)$]	R_1=0.0474 wR_2=0.1231	R_1=0.0526 wR_2=0.1318	R_1=0.0492 wR_2=0.1218	R_1=0.0588 wR_2=0.1355	R_1=0.0542 wR_2=0.0895
Final R indexes [all data]	R_1=0.0507 wR_2=0.1276	R_1=0.0566 wR_2=0.1376	R_1=0.0530 wR_2=0.1266	R_1=0.0652 wR_2=0.1439	R_1=0.1814 wR_2=0.1229
Largest diff. peak/hole (eA^{-3})	0.558/-0.421	0.518/-0.340	0.372/-0.277	0.530/-0.409	0.187/-0.179
CCDC number	2022174	2022175	2022176	2022177	2022178

Table S6. Crystallographic parameters for **3I**

Formula	**$2(C_{24}H_{13}F_4N)\cdot C_6H_{12}N_2$**	**$2(C_{24}H_{13}F_4N)\cdot C_6H_{12}N_2$**	**$2(C_{24}H_{13}F_4N)\cdot C_6H_{12}N_2$**
Formula weight	894.88	894.88	894.88
Temperature (K)	100(2)	200(2)	299(2)
System	monoclinic	monoclinic	monoclinic
Space Group	$P2_1/n$	$P2_1/n$	$P2_1/n$
a (Å)	6.7657(3)	6.7928(4)	6.8192(8)
b (Å)	14.4934(9)	14.5649(8)	14.6728(18)
c (Å)	21.3307(10)	21.3902(12)	21.461(3)
α (°)	90	90	90
β (°)	96.1667(13)	95.7754(16)	95.452(4)
γ (°)	90	90	90
ρ (g/cm^3)	1.429	1.412	1.390
V (Å^3)	2079.54(16)	2105.5(2)	2137.7(5)
Z	2	2	2
Absorption coefficient (mm^{-1})	0.109	0.108	0.106
F(000)	924	924	924
Crystal size (mm)	0.393 x 0.372 x 0.198	0.386 x 0.267 x 0.208	0.393 x 0.372 x 0.198
Radiation [λ (Å)]	MoKα (0.71073)	MoKα (0.71073)	MoKα (0.71073)
Collected reflections	49708	29489	28587
Independent reflections	6833	6161	5098
Data/rest/param	6833/15/356	6161/342/356	5098/15/356
GooF	1.131	1.017	1.009
Final R indexes [$I_0>2\sigma(I_0)$]	R_1=0.0613 wR_2=0.1430	R_1=0.0596 wR_2=0.1075	R_1=0.0572 wR_2=0.1092
Final R indexes [all data]	R_1=0.0755 wR_2=0.1503	R_1=0.1748 wR_2=0.1391	R_1=0.1583 wR_2=0.1405
Largest diff. peak/hole (eA^{-3})	0.435/-0.314	0.199/-0.247	0.158/-0.163
CCDC number	2022179	2022180	2022181

Table S7. Crystallographic parameters for **3II**

Formula	**$2(C_{24}H_{13}F_4N)\cdot C_6H_{12}N_2$**	**$2(C_{24}H_{13}F_4N)\cdot C_6H_{12}N_2$**	**$2(C_{24}H_{13}F_4N)\cdot C_6H_{12}N_2$**	**$2(C_{24}H_{13}F_4N)\cdot C_6H_{12}N_2$**	**$2(C_{24}H_{13}F_4N)\cdot C_6H_{12}N_2$**
Formula weight	894.88	894.88	894.88	894.88	447.44
Temperature (K)	100(2)	150(2)	200(2)	250(2)	300(2)
System	monoclinic	monoclinic	monoclinic	monoclinic	monoclinic
Space Group	Pc	P2/c	P2/c	P2/c	P2/c
a (Å)	19.0865(8)	19.1368(8)	19.1580(7)	19.2225(9)	19.2767(6)
b (Å)	6.7670(3)	6.7789(3)	6.7794(3)	6.7835(3)	6.7799(2)
c (Å)	17.3518(7)	17.4066(8)	17.4666(6)	17.5663(8)	17.6615(6)
α (°)	90	90	90	90	90
β (°)	109.3540(10)	109.3730(10)	109.3620(10)	109.337(2)	109.2900(10)
γ (°)	90	90	90	90	90
ρ (g/cm^3)	1.406	1.395	1.389	1.375	1.364
V (Å^3)	2114.48(16)	2130.24(16)	2140.25(14)	2161.35(17)	2178.66(12)
Z	2	2	2	2	4
Absorption coefficient (mm^{-1})	0.112	0.111	0.111	0.110	0.109
F(000)	924	924	924	924	924
Crystal size (mm)	0.300 x 0.300 x 0.030	0.300 x 0.300 x 0.030	0.300 x 0.300 x 0.030	0.300 x 0.300 x 0.030	0.300 x 0.300 x 0.030
Radiation [λ (Å)]	Synchrotron (0.7288)	Synchrotron (0.7288)	Synchrotron (0.7288)	Synchrotron (0.7288)	Synchrotron (0.7288)
Collected reflections	71153	73488	65803	69239	67379
Independent reflections	12908	6498	6030	5831	5405
Data/rest/param	12908/2/601	6498/75/338	6030/75/338	5831/75/338	5405/75/338
GooF	1.045	1.045	1.034	1.049	1.048
Final R indexes $[I_0>2\sigma(I_0)]$	R_1=0.0381 wR_2=0.0991	R_1=0.0585 wR_2=0.1458	R_1=0.0542 wR_2=0.1407	R_1=0.0572 wR_2=0.1497	R_1=0.0580 wR_2=0.1585
Final R indexes [all data]	R_1=0.0391 wR_2=0.1005	R_1=0.0606 wR_2=0.1484	R_1=0.0585 wR_2=0.1462	R_1=0.0609 wR_2=0.1549	R_1=0.0629 wR_2=0.1661
Largest diff. peak/hole (eA^{-3})	0.498/-0.417	0.863/-0.532	0.666/-0.313	0.462/-0.419	0.375/-0.377
CCDC number	2022182	2022183	2022184	2022185	2022186

Table S8. Crystallographic parameters for **7s**

Formula	**$C_{24}H_{17}N\cdot C_6H_{12}N_2$**
Formula weight	431.56
Temperature (K)	100(2)
System	monoclinic
Space Group	$P2_1/c$
a (Å)	9.1480(4)
b (Å)	22.6374(10)
c (Å)	11.7158(5)
α (°)	90
β (°)	105.813(2)
γ (°)	90
ρ (g/cm^3)	1.228
V (Å^3)	2334.37(10)
Z	4
Absorption coefficient (mm^{-1})	0.075
F(000)	920
Crystal size (mm)	0.250 x 0.110 x 0.005
Radiation [λ (Å)]	Synchrotron (0.7288)
Collected reflections	66651
Independent reflections	7141
Data/rest/param	7141/0/301
GooF	1.027
Final R indexes [$I_0>2\sigma(I_0)$]	R_1=0.0409 wR_2=0.1089
Final R indexes [all data]	R_1=0.0470 wR_2=0.1144
Largest diff. peak/hole (eA^{-3})	0.323/-0.265
CCDC number	2022187

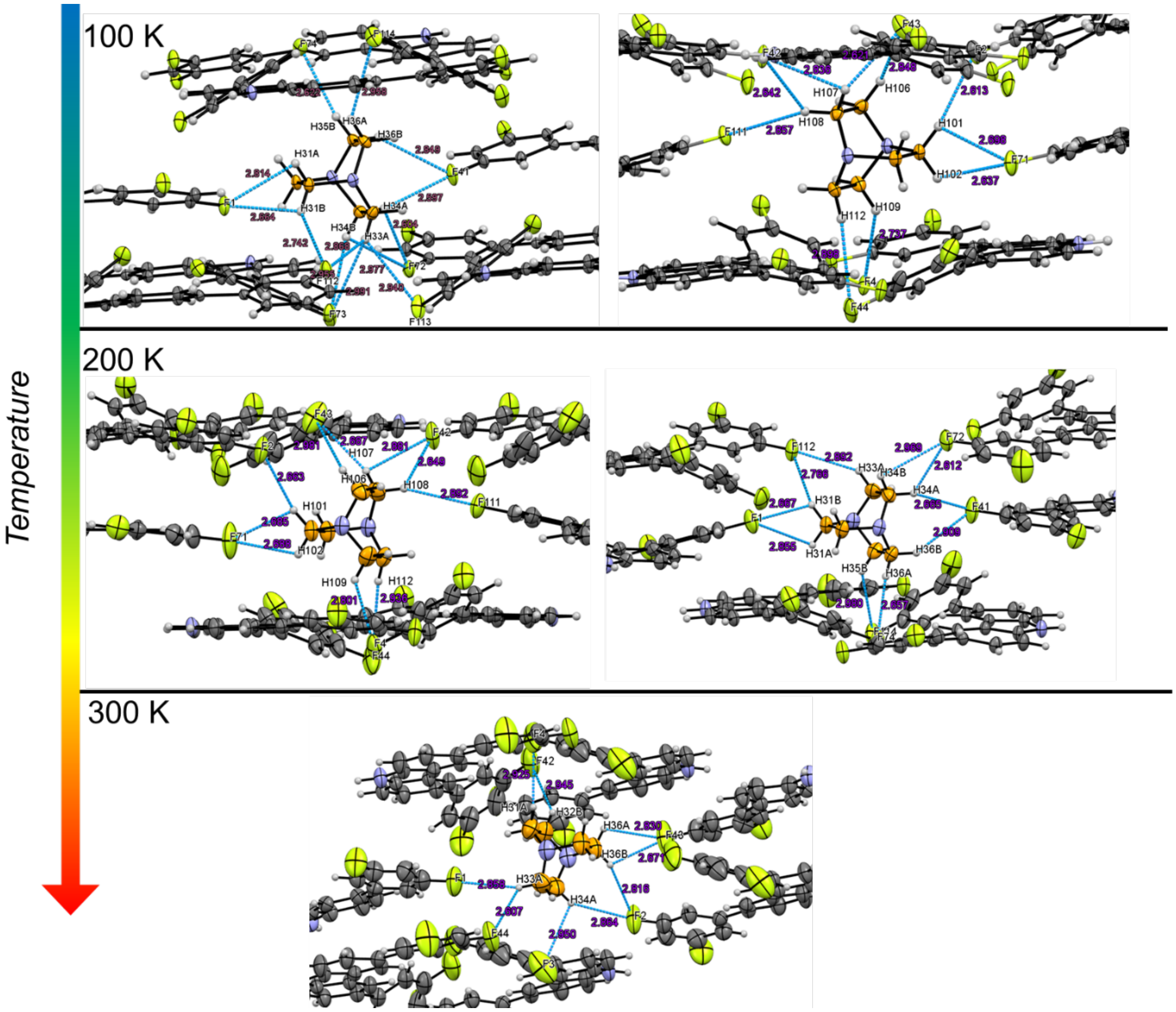

Figure S24. Interactions C-H···F-C around DABCO in rotor **1** at different temperatures (ORTEP diagram, 50% level probability). For structures at 100 and 200 K (**1-LT**) are shown both DABCO fragments in the asymmetric unit, the hydrogen bonded carbazole units were omitted.

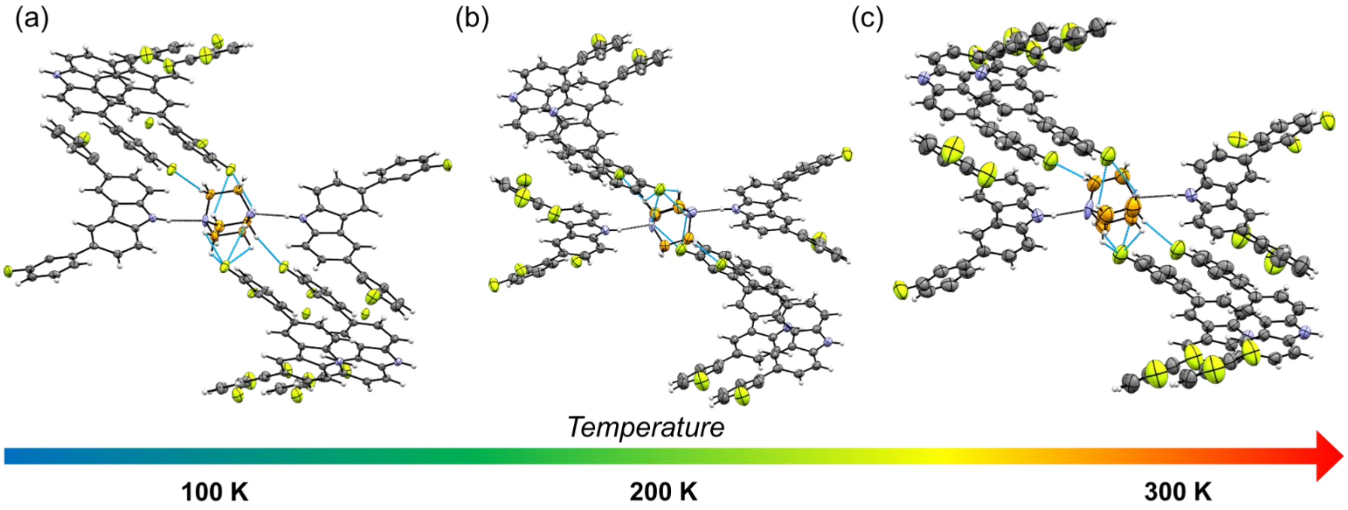

Figure S25. Crystal arrangement of cocrystal **3I** (ORTEP diagram, 50% level probability). Close interactions C-F···H-C around DABCO are highlighted with blue dotted lines.

Table S9. Close contacts C-H···F-C present around DABCO in rotor **1** at several temperatures per unit cell

Rotor 1					
Experimental (100K)		**Optimization (100 K)**		**Experimental (300 K)**	
F1-H31A	2.814	**F1-H**	2.467	**F1-H31A**	2.855
F1-H31B	2.664	**F1-H**	2.667	**F1-31B**	2.667
F41-H34A	2.597	**F2-H**	2.881	**F41-34A**	2.665
F41-H36B	2.849	**F3-H**	2.930	**F41-H36B**	2.909
F72-H34A	2.604	**F3-H**	2.930	**F72-H34A**	2.612
F72-H34B	2.94	**F4-H**	2.713	**F72-H34B**	2.969
F73-H33A	2.991	**F4-H**	2.602	**F74-H36A**	2.657
F73-H34B	2.955	**F5-H**	2.578	**F112-H31B**	2.766
F74-H36A	2.622	**F5-H**	2.734	**F112-H33B**	2.892
F113-H33A	2.977	**F6-H**	2.899	**F114-H35B**	2.98
F112-H31B	2.742	**F7-H**	2.667	**F4-H109**	2.801
F112-H33A	2.868	**F7-H**	2.467	**F2-H101**	2.663
F114-H35B	2.958	**F8-H**	2.489	**F44-H112**	2.936
F4-H109	2.737	**F9-H**	2.734	**F43-H106**	2.981
F2-H101	2.613	**F9-H**	2.578	**F43-H107**	2.687
F44-H112	2.898	**F10-H**	2.61	**F42-H107**	2.881
F43-H106	2.848	**F11-H**	2.92	**F42-H108**	2.649
F43-H107	2.621	**F11-H**	2.93	**F71-H101**	2.685
F42-H107	2.836	**F12-H**	2.518	**F71-H102**	2.688
F42H108	2.642	**F12-H**	2.902	**F111-H108**	2.892
F71-H101	2.698	**F13-H**	2.701	**F1-H31A**	2.855
F71-H102	2.637	**F13-H**	2.862	**F1-31B**	2.667
F111-H108	2.857	**F14-H**	2.548	**F41-34A**	2.665
F1-H31A	2.814	**F14-H**	2.763	**F41-H36B**	2.909
F1-H31B	2.664	**F15-H**	2.518	**F72-H34A**	2.612
F41-H34A	2.597	**F15-H**	2.746	**F72-H34B**	2.969
F41-H36B	2.849	**F16-H**	2.714	**F74-H36A**	2.657
F72-H34A	2.604	**F16-H**	2.59	**F112-H31B**	2.766
F72-H34B	2.94	**F17-H**	2.794	**F112-H33B**	2.892
F73-H33A	2.991	**F18-H**	2.63	**F114-H35B**	2.98
F73-H34B	2.955	**F19-H**	2.59	**F4-H109**	2.801
F74-H36A	2.622	**F19-H**	2.71	**F2-H101**	2.663
F113-H33A	2.977	**F20-H**	2.79	**F44-H112**	2.936
F112-H31B	2.742	**F21-H**	2.63	**F43-H106**	2.981
F112-H33A	2.868	**F22-H**	2.862	**F43-H107**	2.687
F114-H35B	2.958	**F22-H**	2.701	**F42-H107**	2.881
F4-H109	2.737	**F23-H**	2.549	**F42-H108**	2.649
F2-H101	2.613	**F23-H**	2.770	**F71-H101**	2.685
F44-H112	2.898	**F24-H**	2.755	**F71-H102**	2.688
F43-H106	2.848	**F24-H**	2.51	**F111-H108**	2.892
F43-H107	2.621				
F42-H107	2.836				
F42H108	2.642				
F71-H101	2.698				
F71-H102	2.637				
F111-H108	2.857				

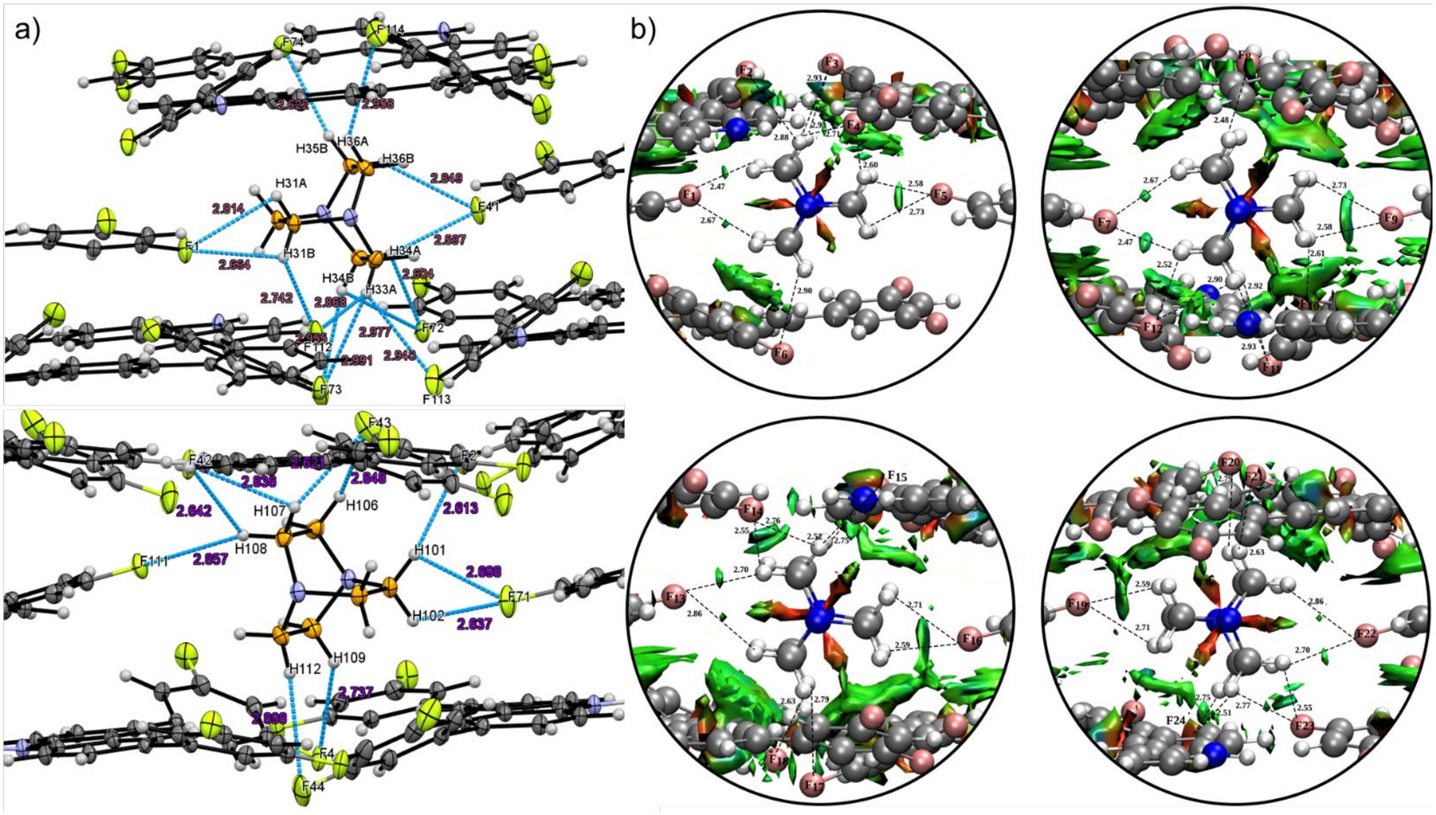

Figure S26. Comparative between contacts showed by a) XRD data and b) optimized structures in rotor **1**, both at 100 K. For a) the two DABCO units showed are present in the asymmetric unit at that temperature.

Table S10. Close contacts C-H···F-C present around DABCO in rotor **2** at several temperatures per unit cell

Rotor 2					
Experimental (100 K)		**Optimization (100 K)**		**Experimental (300 K)**	
F2-H27B	2.824	**F1-H**	2.770	**F2-H29A**	2.968
F2-H30A	2.723	**F2-H**	2.583	**F2-H29B**	2.678
F2-H27B	2.824	**F2-H**	2.772	**F2-H30A**	2.861
F2-H30A	2.723	**F2-H**	2.639	**F2-H30B**	2.993
F4-H25B	2.793	**F2-H**	2.572	**F3-H27B**	2.859
F4-H26A	2.853	**F2-H**	2.773	**F2-H25A**	2.756
F4-H29B	2.92	**F3-H**	2.689	**F2-H28B**	2.645
F4-H29A	2.612	**F4-H**	2.889	**F3-H30B**	2.988
F4-H26B	2.646	**F4-H**	2.976	**F2-H26A**	2.945
F4-H27A	2.858	**F4-H**	2.701	**F2-H29A**	2.968
F4-H27B	2.64	**F4-H**	2.847	**F2-H29B**	2.678
F4-H28A	2.704	**F4-H**	2.464	**F2-H30A**	2.861
F4-H28B	2.818	**F5-H**	2.823	**F2-H30B**	2.993
F4-H25B	2.793	**F5-H**	2.978	**F3-H27B**	2.859
F4-H26A	2.853	**F5-H**	2.561	**F2-H25A**	2.756
F4-H29B	2.92	**F5-H**	2.622	**F2-H28B**	2.645
F4-H29A	2.612	**F5-H**	2.452	**F3-H30B**	2.988
F4-H26B	2.646	**F6-H**	2.612	**F2-H26A**	2.945
F4-H27A	2.858	**F6-H**	2.469		
F4-H27B	2.64	**F6-H**	2.605		
F4-H28A	2.704				
F4-H28B	2.818				

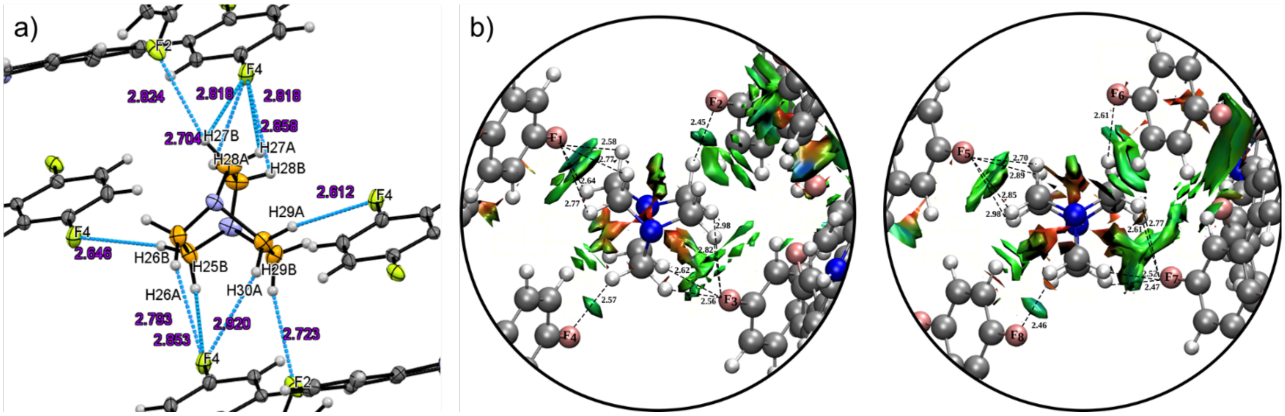

Figure S27. Comparative between contacts showed by a) XRD data and b) optimized structures in rotor **2**, both at 100 K.

Table S11. Close contacts C-H···F-C present around DABCO in rotor **3I** at several temperatures per unit cell

Rotor 3I					
Experimental (100 K)		**Optimization (100 K)**		**Experimental (300 K)**	
F4-H27A	2.671	**F1-H**	2.601	**F4-H27A**	2.823
F4-H27B	2.735	**F1-H**	2.773	**F4-H27B**	2.749
F4-H28A	2.619	**F1-H**	2.930	**F4-H28A**	2.598
F4-H28B	2.524	**F1-H**	2.595	**F4-H28B**	2.804
F4-H25A	2.676	**F2-H**	2.269	**F4-H29B**	2.78
F4-H30A	2.628	**F3-H**	2.777	**F4-H26B**	2.725
F4-H25B	2.816	**F4-H**	2.679	**F4-H29A**	2.918
F4-H26A	2.863	**F4-H**	2.911	**F4-H30A**	2.959
F4-H27A	2.671	**F4-H**	2.629	**F4-H27A**	2.823
F4-H27B	2.735	**F5-H**	2.224	**F4-H27B**	2.749
F4-H28A	2.619	**F6-H**	2.724	**F4-H28A**	2.598
F4-H28B	2.524	**F7-H**	2.268	**F4-H28B**	2.804
F4-H25A	2.676	**F8-H**	2.773	**F4-H29B**	2.78
F4-H30A	2.628	**F8-H**	2.938	**F4-H26B**	2.725
F4-H25B	2.816	**F8-H**	2.595	**F4-H29A**	2.918
F4-H26A	2.863	**F8-H**	2.601	**F4-H30A**	2.959
		F9-H	2.679		
		F10-H	2.225		
		F11-H	2.630		
		F11-H	2.724		

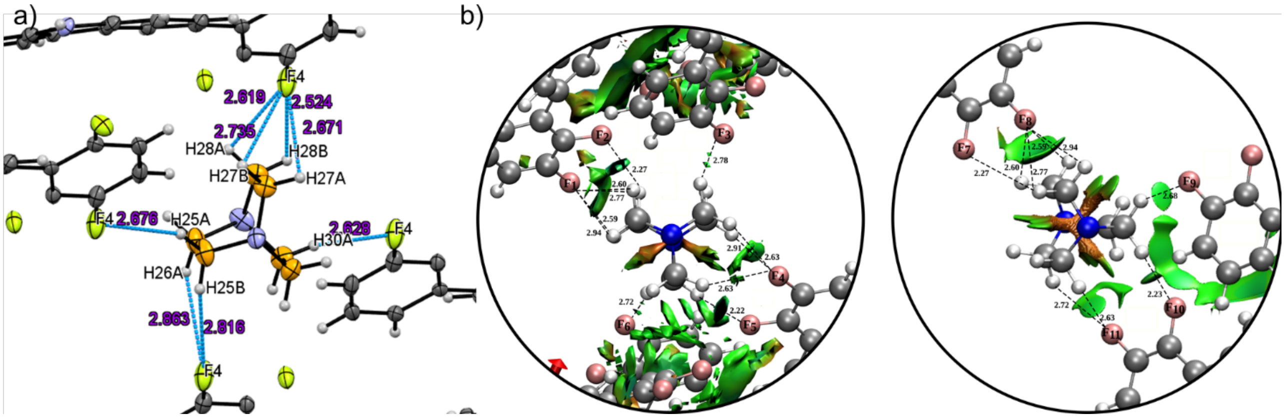

Figure S28. Comparative between contacts showed by a) XRD data and b) optimized structures in rotor **3I**, both at 100 K.

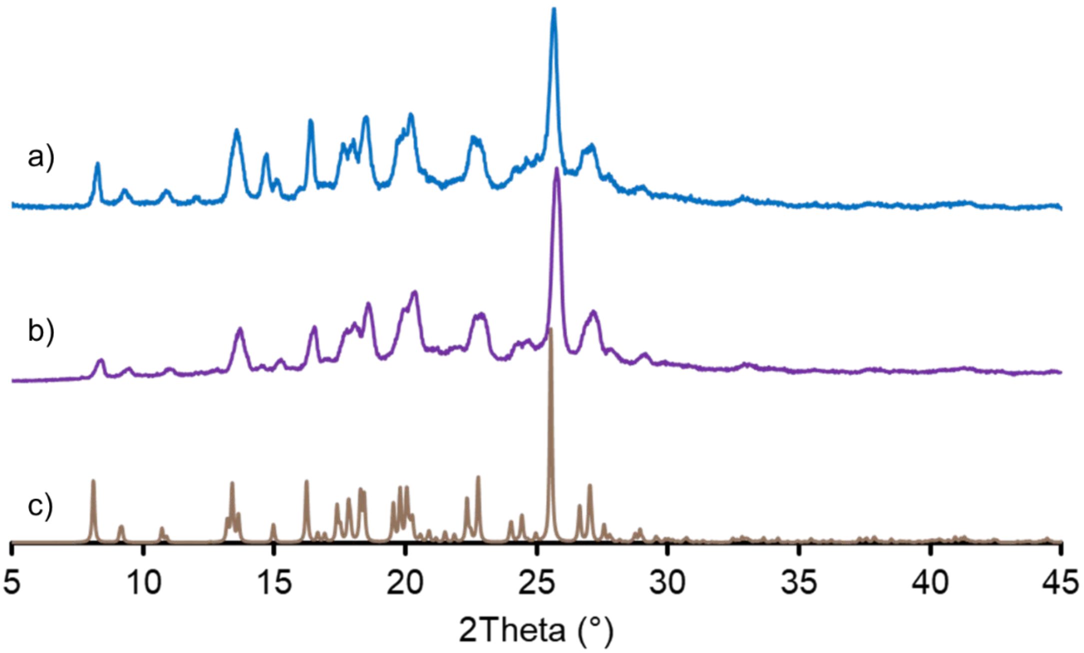

Figure S29. Comparison of Powder X-Ray diffraction patterns: **a) 1-*d*$_{10}$** experimental, **b) 1** experimental and **c)** Calculated from **1**

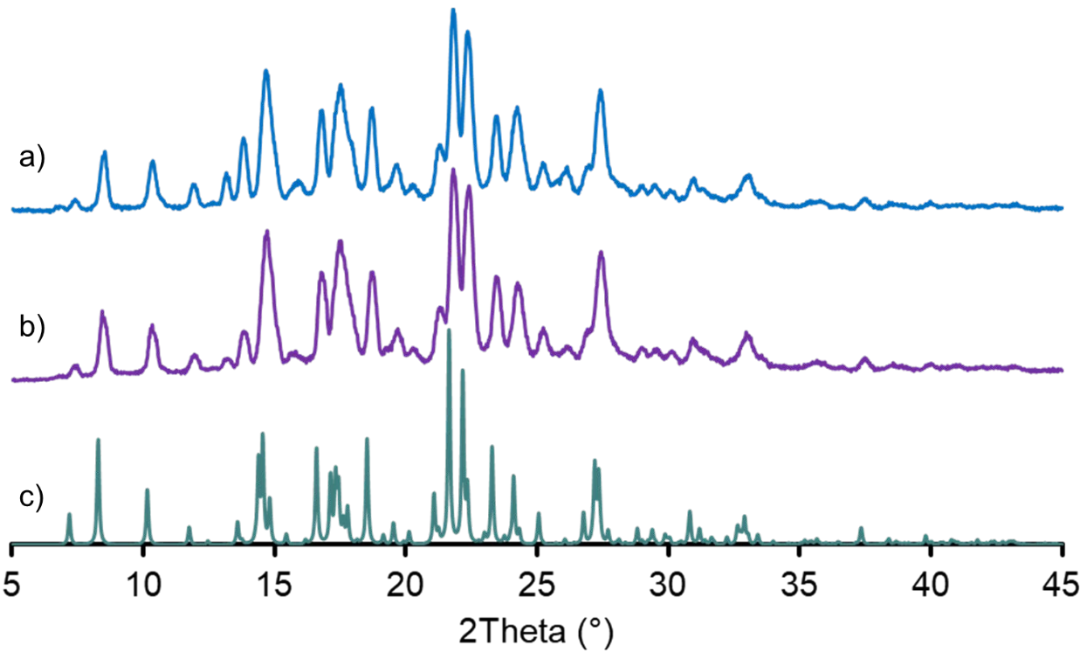

Figure S30. Comparison of Powder X-Ray diffraction patterns: **a) 2-*d*$_{10}$** experimental, **b) 2** experimental and **c)** Calculated from **2**

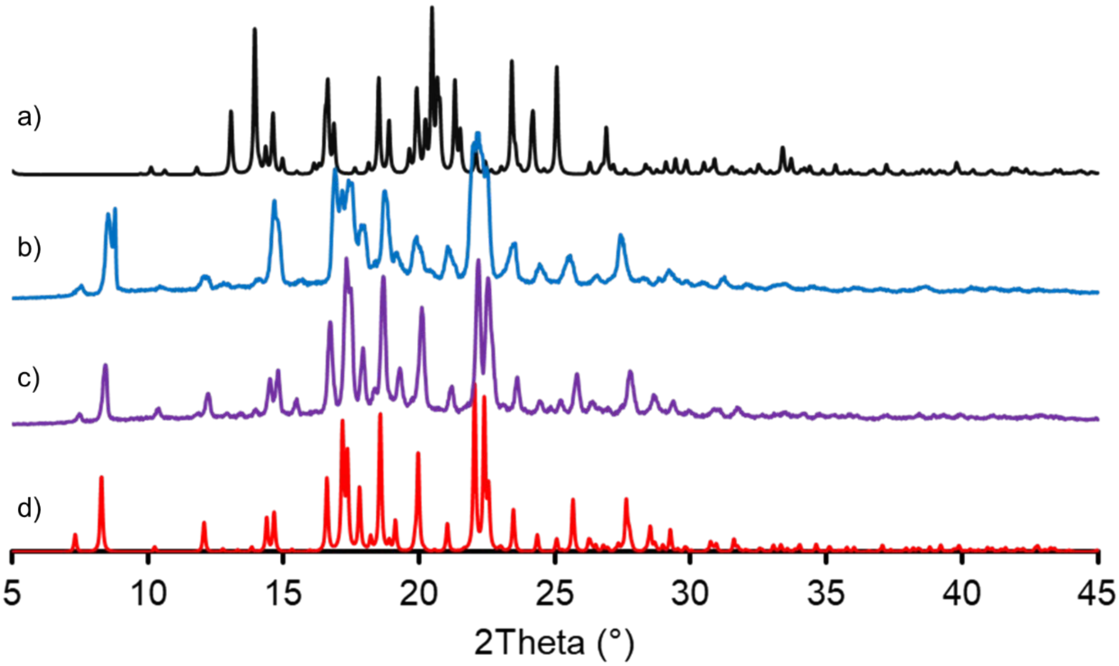

Figure S31. Comparison of Powder X-Ray diffraction patterns. **a)** Calculated from **3II**, **b) 3I-*d*$_{10}$** experimental, **c) 3I** experimental and **d)** calculated from **3I**

Solid-state ^{13}C CPMAS

^{13}C NMR CPMAS spectra was recorded according with conditions described using polycrystalline samples of cocrystals in a Bruker Avance 500 with a PH MAS DVT 500S1 BL3.2 probe at spectrometer frequency of 125.78 MHz and room temperature (300 K) for all experiments. In following figures, signals marked "*" are assigned for carbon atoms of DABCO.

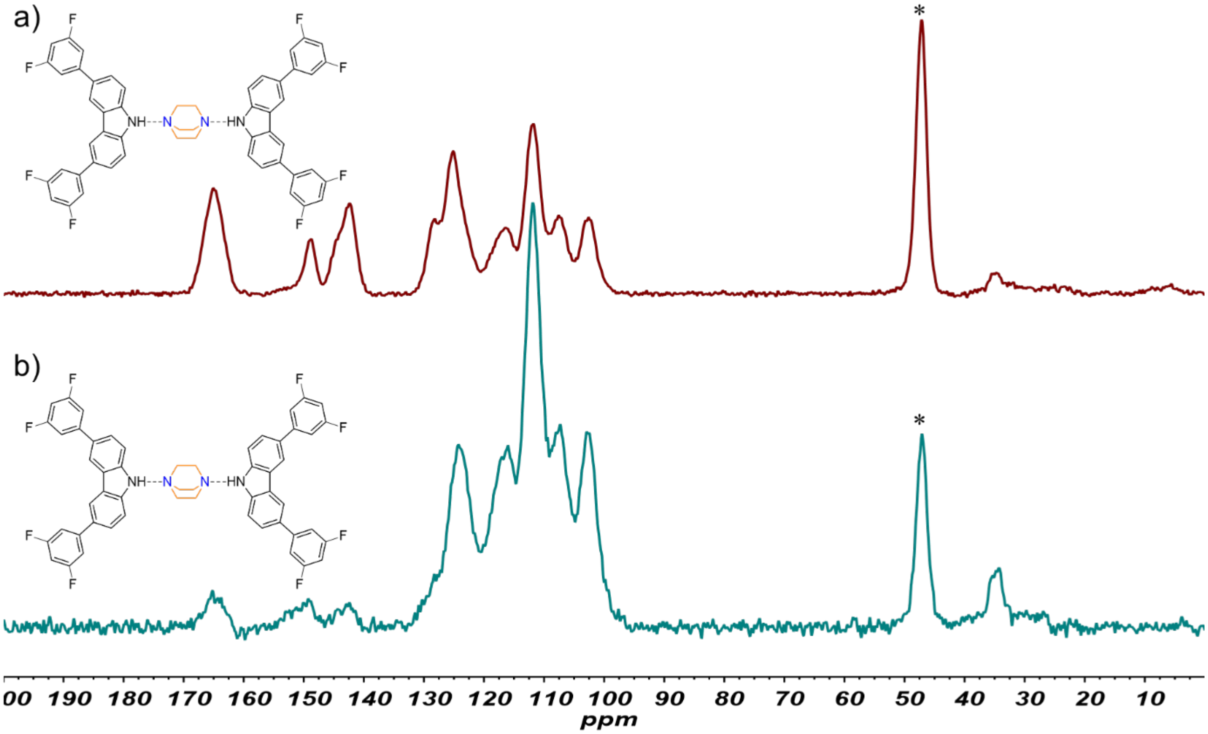

Figure S32. ^{13}C CPMAS spectra of a) rotor **1** (d_1 = 20 s, p_{15} = 2.5 ms, 15 kHz spinning) and b) rotor **1** (d_1 = 20 s, p_{15} = 0.1 ms, 15 kHz spinning).

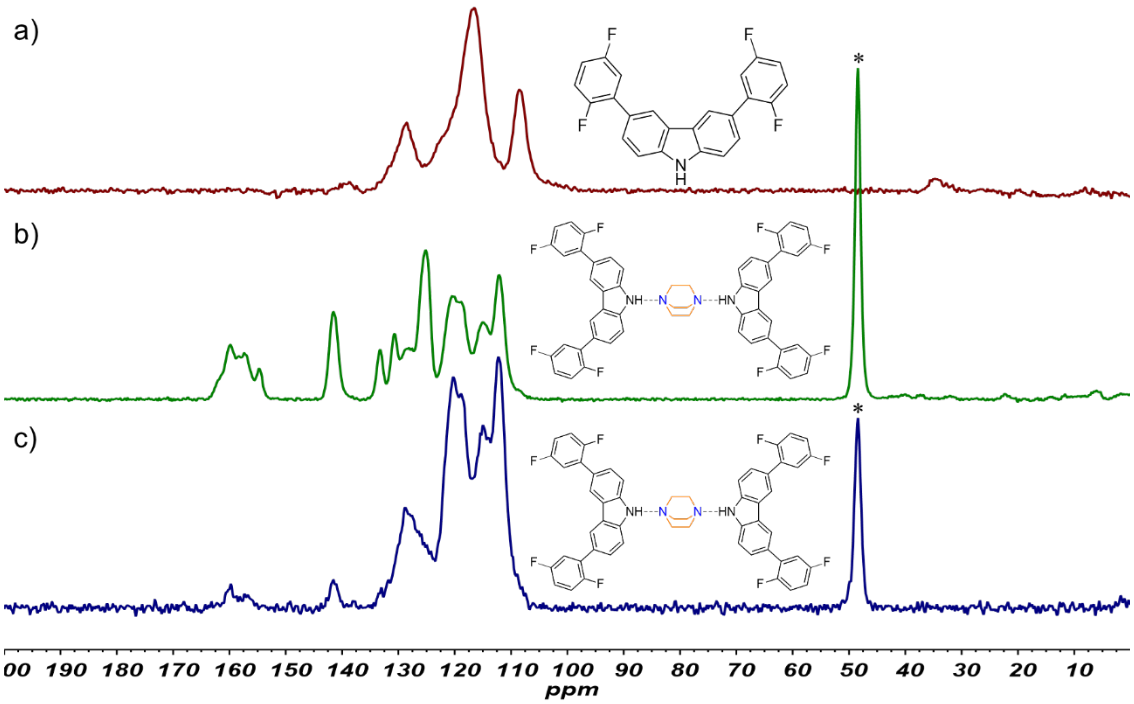

Figure S33. ^{13}C CPMAS spectra of a) compound **5** (d_1 = 20 s, p_{15} = 2.5 ms, 15 kHz spinning), b) rotor **2** (d_1 = 20 s, p_{15} = 2.5 ms, 15 kHz spinning) and c) rotor **2** (d_1 = 20 s, p_{15} = 0.1 ms, 15 kHz spinning).

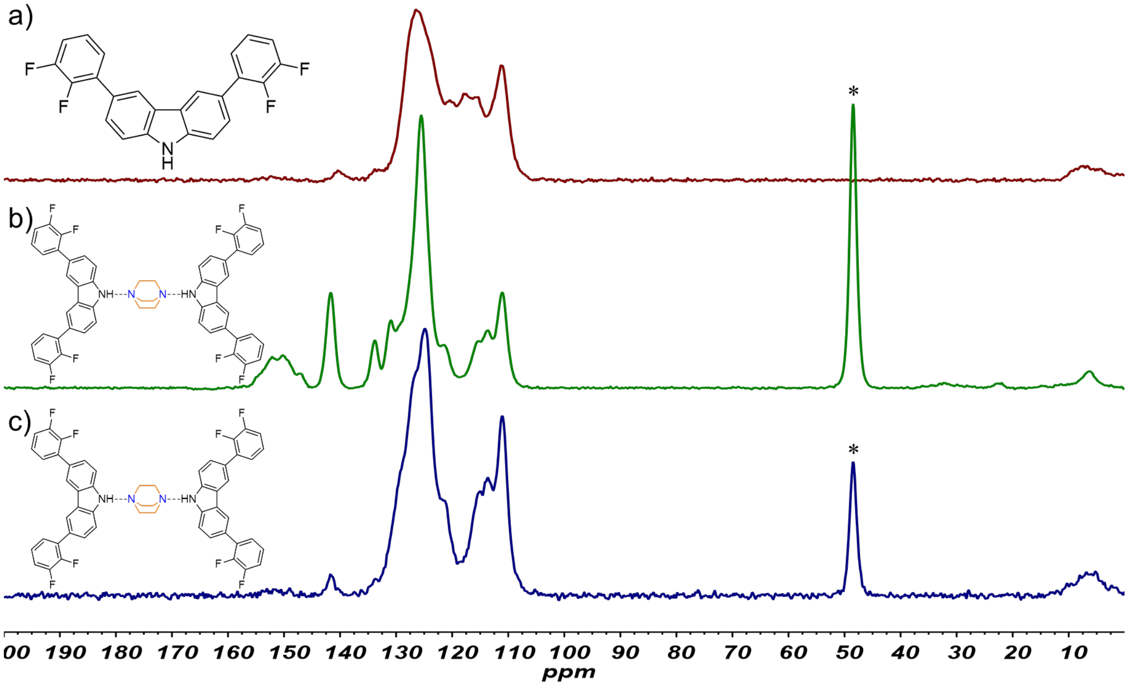

Figure S34. ^{13}C CPMAS spectra of a) compound **6** (d_1 = 20 s, p_{15} = 2.5 ms, 15 kHz spinning), b) rotor **3I** (d_1 = 20 s, p_{15} = 2.5 ms, 15 kHz spinning) and c) rotor **3I** (d_1 = 20 s, p_{15} = 0.1 ms, 15 kHz spinning).

VT ^{2}H Echo-spin experiments

Solid-state ^{2}H echo-spin experiments were performed on a Bruker AV600 instrument at 92.1 MHz (deuterium resonance frequency) with a 5 mm wideline probe and 90-degree pulse of 2.9 µs. To suppress the undesired artifacts, a quadrupolar-echo sequence with phase recycling was used. An echo delay of 50 µs was used after the refocusing delay of 46 µs, and the recycle delay between pulses was 5 s. In the experiment, about 50 mg of sample was placed in a short borosilicate glass NMR tube. 256 scans were acquired for all temperatures explored. All spectra in this work were obtained using a line broadening of 3.0 kHz in data processing.

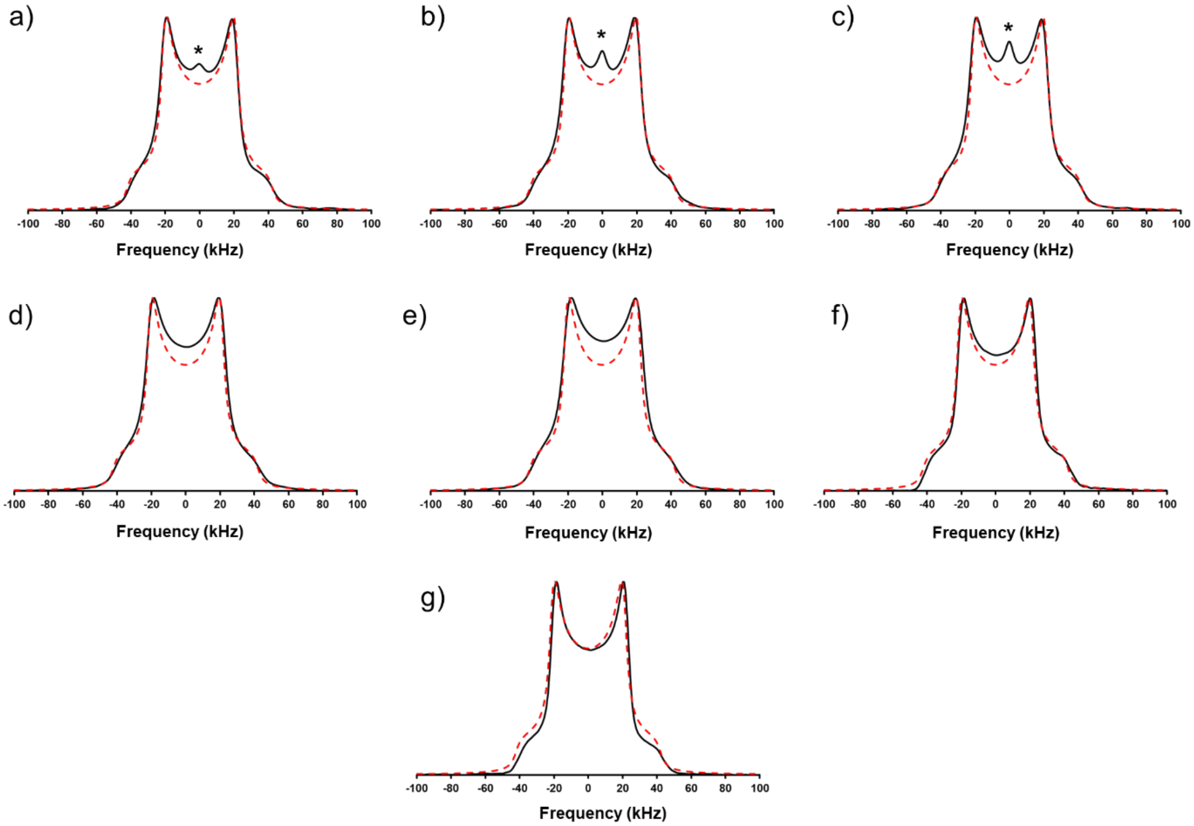

Figure S35. Variable temperature ^{2}H quadrupolar echo-spin spectra of rotor **1-*d*$_{10}$**. In this order: a) 350 K, b) 325 K, c) 300 K, d) 250 K, e) 200 K, f) 175 K and g) 150 K. Experimental data is shown in black and simulated in red dotted lines. For simulated data were used a QCC of 170 kHz, cone angle of 70° and line-broadening of 6 kHz. "*" shows the signal assigned for isotropic motion of free DABCO.

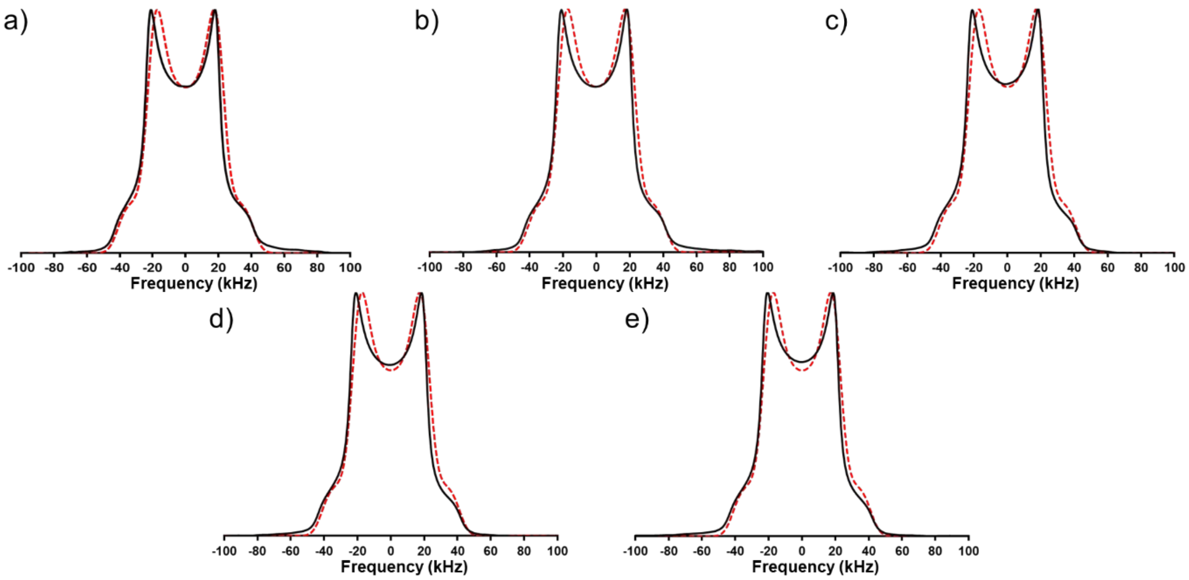

Figure S36. Variable temperature ^{2}H quadrupolar echo-spin spectra of rotor **2-*d*$_{10}$**. In this order: a) 300 K, b) 250 K, c) 200 K, d) 175 K, e) 150 K. Experimental data is shown in black and simulated in red dotted lines. For simulated data were used a QCC of 170 kHz, cone angle of 70° and line-broadening of 6 kHz.

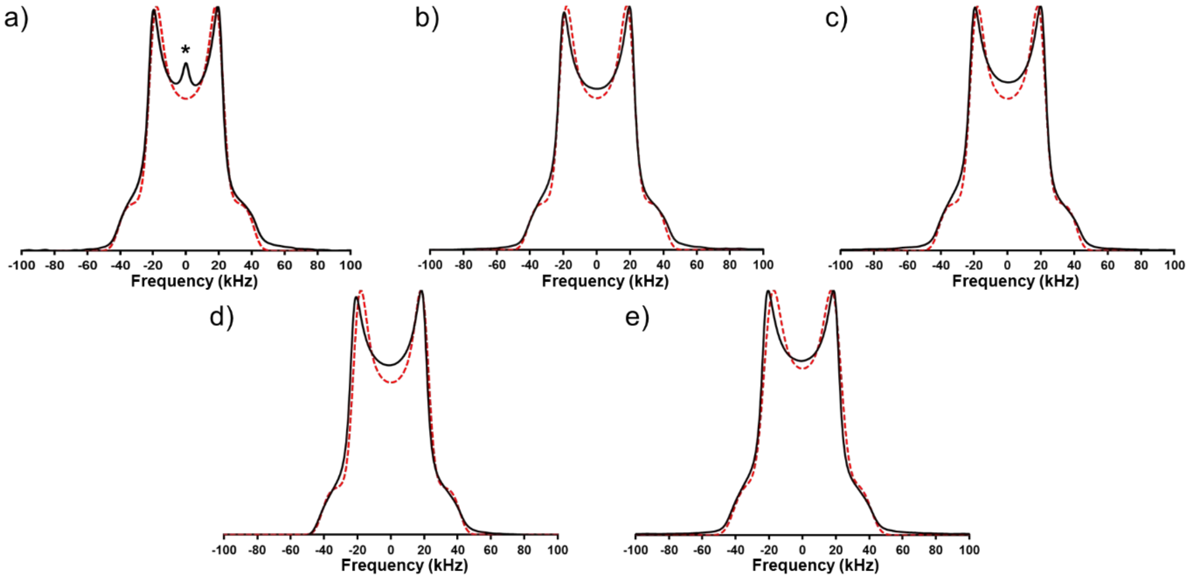

Figure S37. Variable temperature ^{2}H quadrupolar echo-spin spectra of rotor **3I-*d*$_{10}$**. In this order: a) 300 K, b) 250 K, c) 200 K, d) 175 K, e) 150 K. Experimental data is shown in black and simulated in red dotted lines. For simulated data were used a QCC of 170 kHz, cone angle of 70° and line-broadening of 6 kHz. "*" shows the signal assigned for isotropic motion of free DABCO.

Computational section

DFT periodic computations were carried out by using the Vienna ab initio simulation package (VASP 5.4.4)[S8],[S9] with the projector augmented wave (PAW) potentials to describe the interaction between ions and electrons.[S10] The generalized gradient approximation, as proposed by Perdew-Burke-Ernzerhof (PBE-GGA),[S11] is used for the exchange and correlation potential in conjunction with the Grimme's D3-dispersion correction approach.[S12] The plane-wave kinetic-energy cutoff is set at 600 eV. The first Brillouin zone was sampling using Monkhorst-Pack k-grids of 4×2×1 and 2×2×1 k-points. The lattice parameters of each system were obtained by direct minimization of the total energy, with the atomic positions fully optimized until the interatomic forces were less than 0.001 eV/Å. Energy barriers were calculated using the Nudged Elastic Band (NEB)[S13] method implemented in VASP. The calculation was initialized using by seven intermediate images on each path segment, obtained by cubic spline interpolation. All NEB calculations were done for a fixed cell shape and volume.

Structural parameters

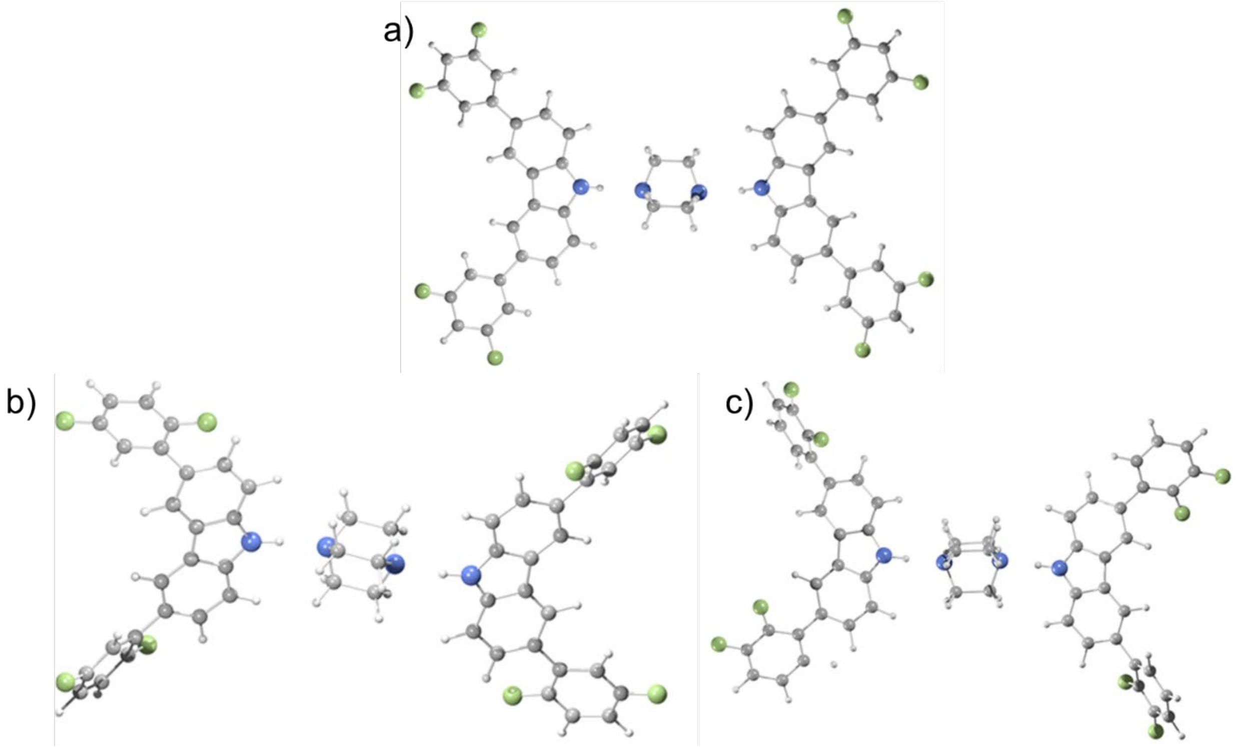

Figure S38. Atomic representation of optimized rotors a) **1**, b) **2** and c) **3I**. For the modelling of these structures, single crystal data at 100 K was used.

Table S12. Comparative table of calculated and experimental cell parameters for cocrystals.

Lattice parameter	Method	1-LT (100 K)	1-LT (200 K)	1-HT (300 K)	2 (100 K)	3I (100 K)
a (Å)	Experimental	14.018	14.044	13.952	6.657	6.766
	Calculated	14.013	14.001	13.630	6.605	6.748
	% Error	(0.04 %)	(0.31 %)	(2.31 %)	(0.78 %)	(0.27 %)
b (Å)	Experimental	13.633	13.774	14.094	14.852	14.493
	Calculated	13.733	13.732	14.052	14.904	14.441
	% Error	(0.73 %)	(0.30 %)	(0.30 %)	(0.35 %)	(0.36 %)
c (Å)	Experimental	22.765	22.842	22.779	21.254	21.331
	Calculated	22.479	22.480	22.489	20.869	21.059
	% Error	(1.26 %)	(1.58 %)	(1.27 %)	(1.81 %)	(1.28 %)
α (°)	Experimental	90.0	90.0	90.0	90.0	90.0
	Calculated	90.0	90.0	90.0	90	90.0
	% Error	(0.0 %)	(0.0 %)	(0.0 %)	(0.0 %)	(0.0 %)
β (°)	Experimental	107.54	107.6	106.4	95.72	96.2
	Calculated	107.70	107.7	106.4	96.96	97.1
	% Error	(0.15 %)	(0.1 %)	(0.0 %)	(1.30 %)	(0.94 %)
γ (°)	Experimental	90.0	90.0	90.0	90.0	90.0
	Calculated	90.0	90.0	90.0	90.0	90.0
	% Error	(0.0 %)	(0.0 %)	(0.0 %)	(0.0 %)	(0.0 %)
Volume (Å^3)	Experimental	4148.216	4212.210	4296.547	2090.882	2079.542
	Calculated	4121.157	4117.928	4133.111	2030.241	2036.345
	% Error	(0.65 %)	(2.24 %)	(3.80 %)	(2.90 %)	(2.08 %)

Rotational barriers

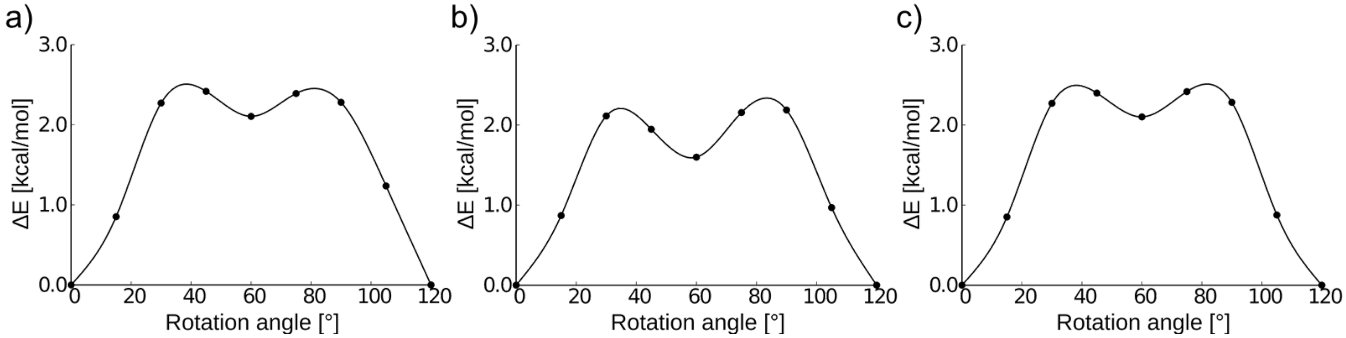

Figure S39. Calculated rotational barriers for rotor **1** at a) 100 K, b) 200 K and c) 300 K. Maximum at 2.5, 2.4 and 2.3 kcal/mol, respectively.

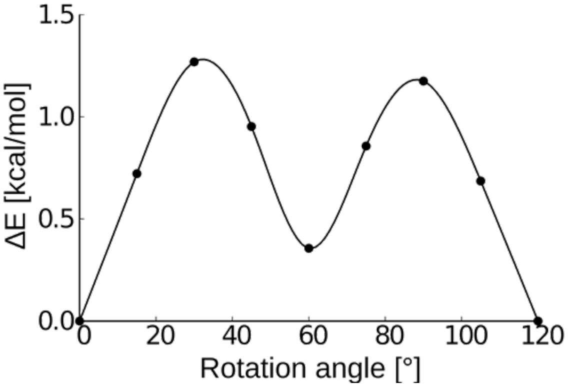

Figure S40. Calculated rotational barrier for rotor **2** at 100 K. Maximum at 1.3 kcal/mol.

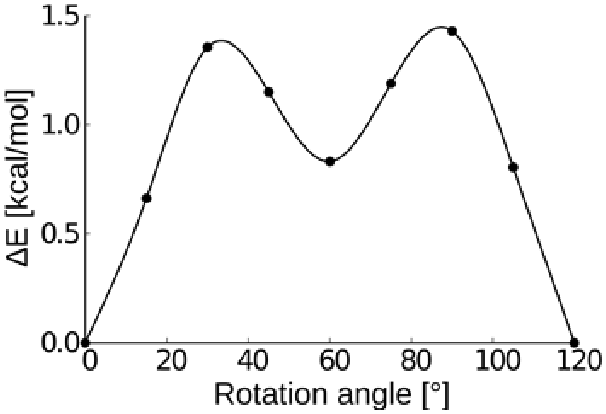

Figure S41. Calculated rotational barrier for rotor **3I** at 100 K. Maximum at 1.4 kcal/mol.

Non-covalent interactions

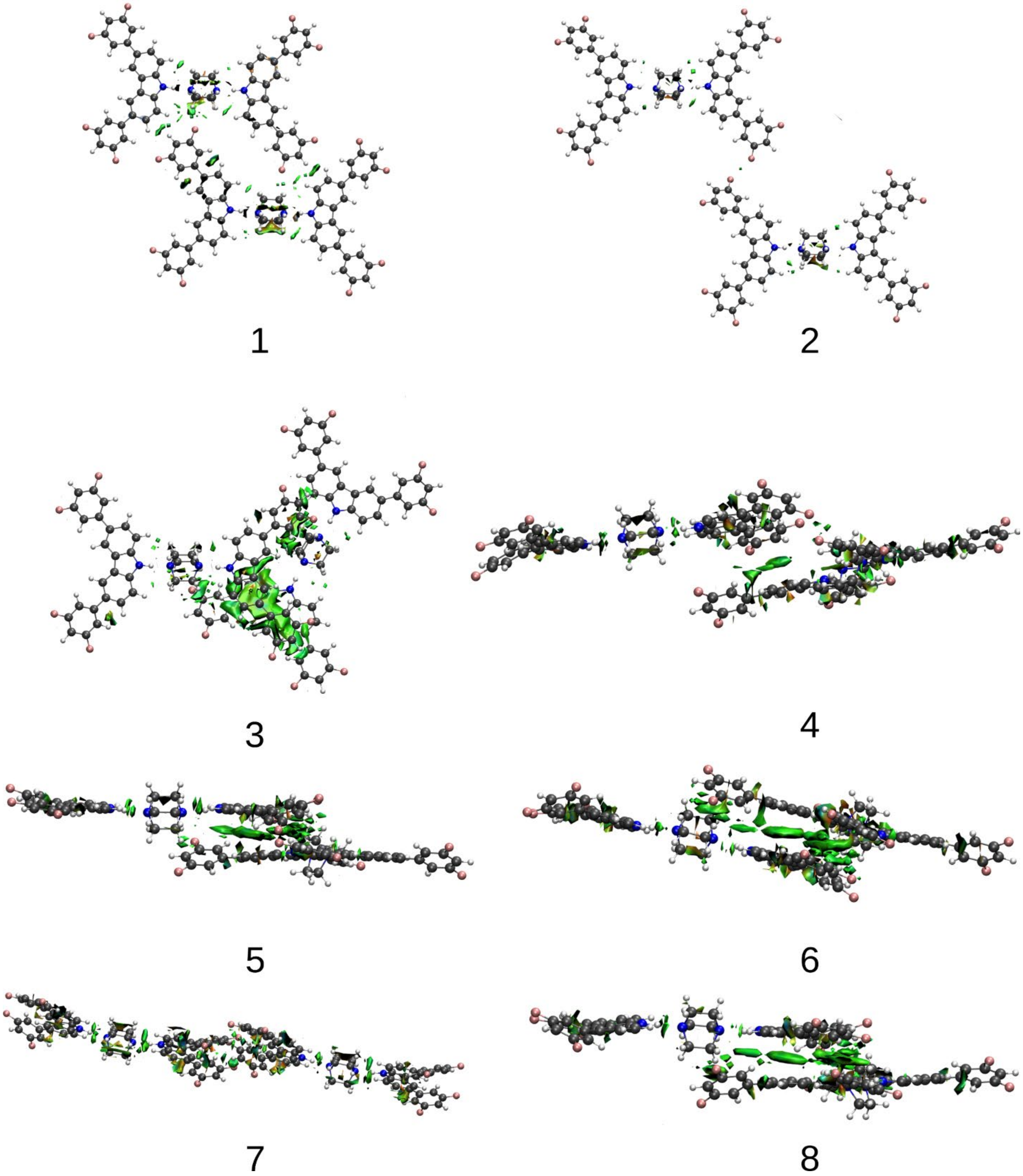

Figure S42. Non-covalent interactions (NCIs) analyses. Plots in pairs found in **1-LT**.

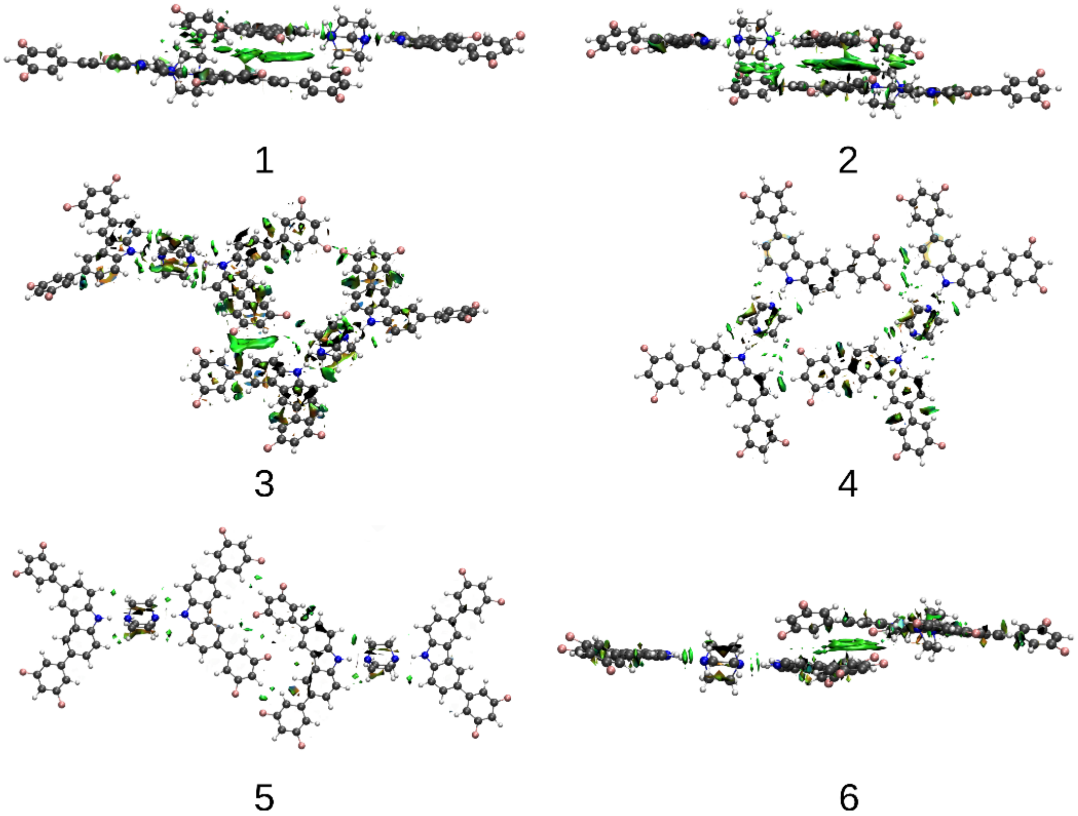

Figure S43. Non-covalent interactions (NCIs) analyses. Plots in pairs found in **1-HT**.

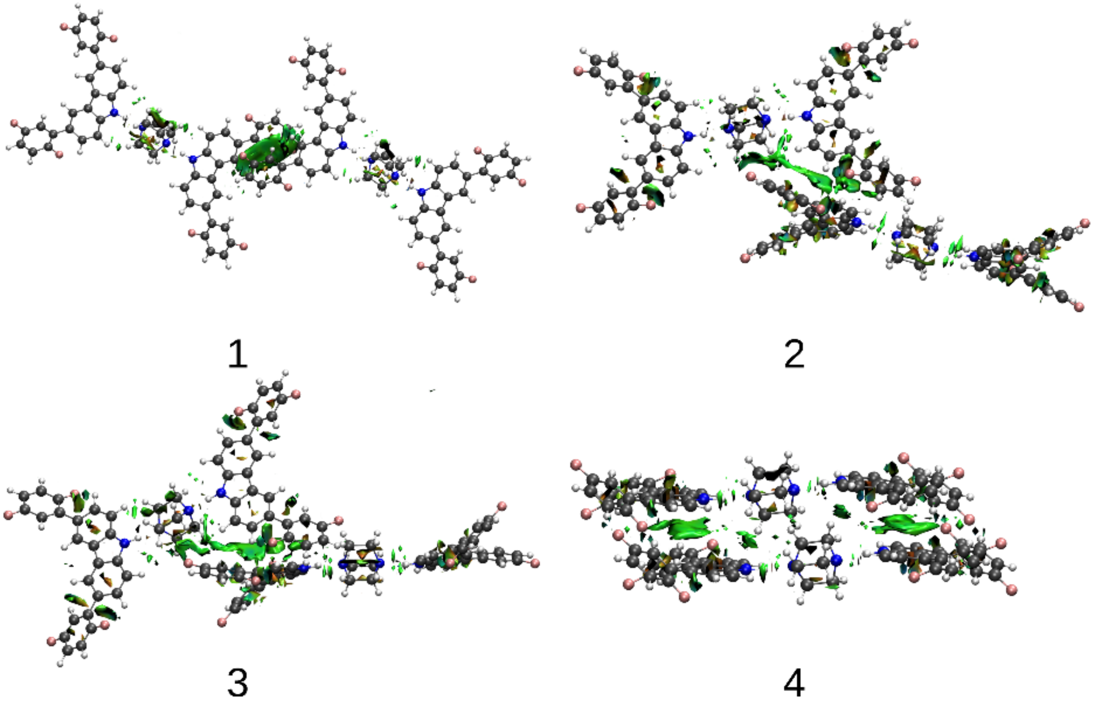

Figure S44. Non-covalent interactions (NCIs) analyses. Plots in pairs found in **2**.

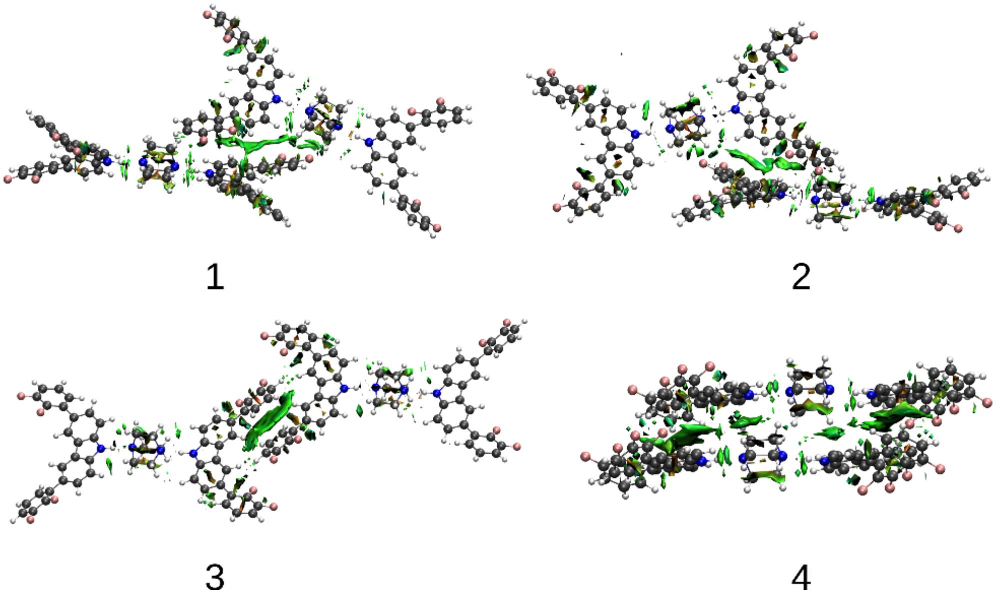

Figure S45. Non-covalent interactions (NCIs) analyses. Plots in pairs found in **3I**.

VT ^{1}H and T_1 spin-lattice relaxation experiments

T_1 experiments were performed on a Bruker AV600 instrument set at 600 MHz with a saturation-recovery pulse sequence featuring a delay time *t* between two 90º pulses. The intensity of wideline ^{1}H NMR spectrum was monitored, and a set of delay time was used for each sample at different temperatures to ensure the sufficient recovery of spectrum intensity (approximately 5 × T_1). Crystalline powder of the samples was placed in a short borosilicate tube (cut from a regular 5-mm NMR tube) capped with Teflon plugs at both ends. T_1 data was obtained from exponential fitting of the spectrum intensity change as a function of *t*.

$$I(t) = I_0\left[1\text{-}e^{-\frac{t}{T_1}}\right]$$

Table S13. Summarized T_1 data for rotors

1		**2**		**3I**	
1000/T	**ln(T_1^{-1})**	**1000/T**	**ln(T_1^{-1})**	**1000/T**	**ln(T_1^{-1})**
2.86	-0.774036	3.33333	-2.27187	3.33333	-1.75279
3.08	-0.601416	3.63636	-2.27869	3.63636	-1.66055
3.33	-0.499259	4	-2.18619	4	-1.48256
3.63636	-0.413962	4.44444	-2.0408	4.44444	-1.26805
4	-0.565882	5	-1.84202	5	-1.05536
4.44444	-0.937191	5.71429	-1.51978	5.71429	-0.750756
5	-1.40984	6.66667	-1.07179	6.66667	-0.512464

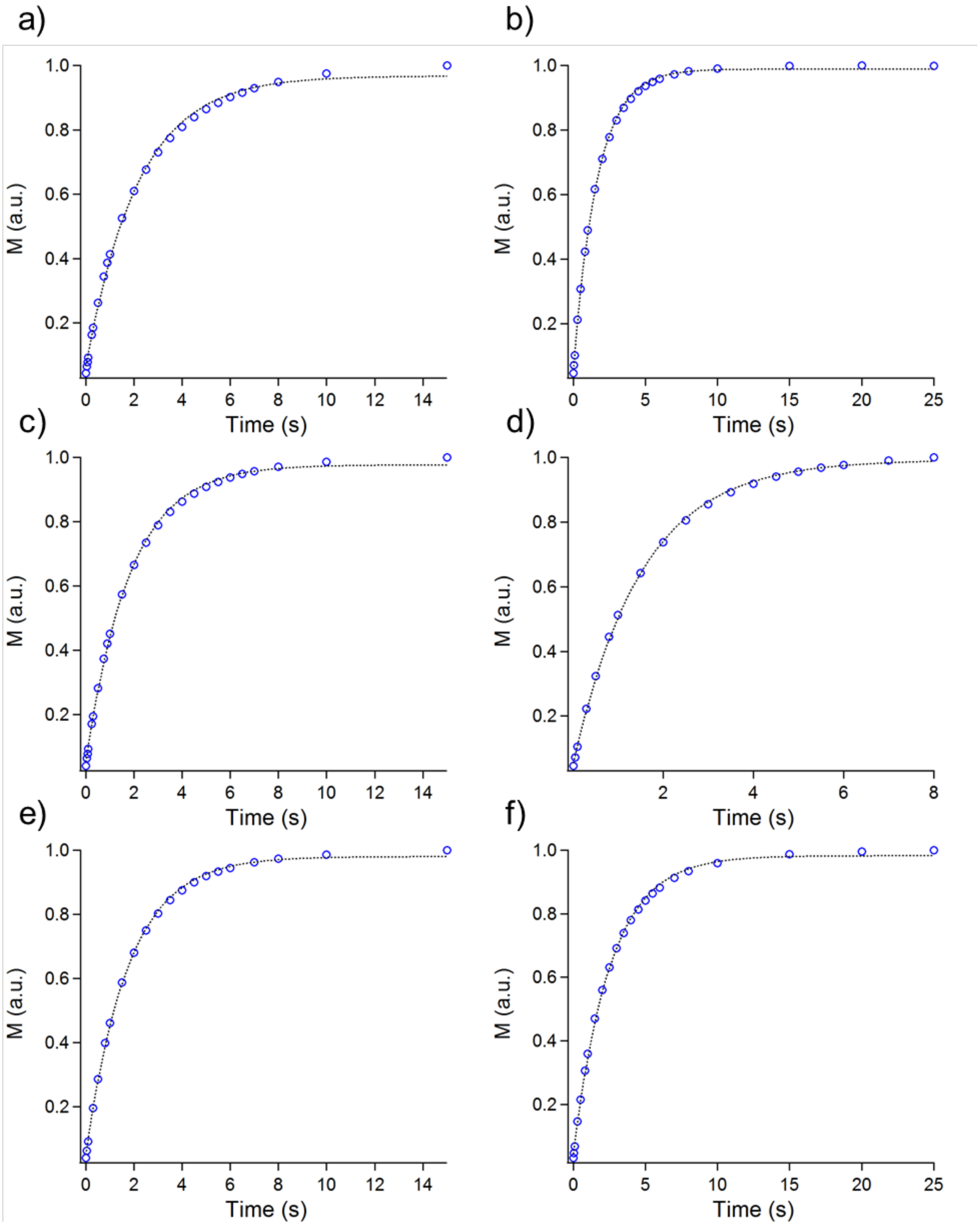

Figure S46. Fitting of saturation recovery data for **1** at a) 350, b) 325, c) 300, d) 275, e) 250 and f) 225 K

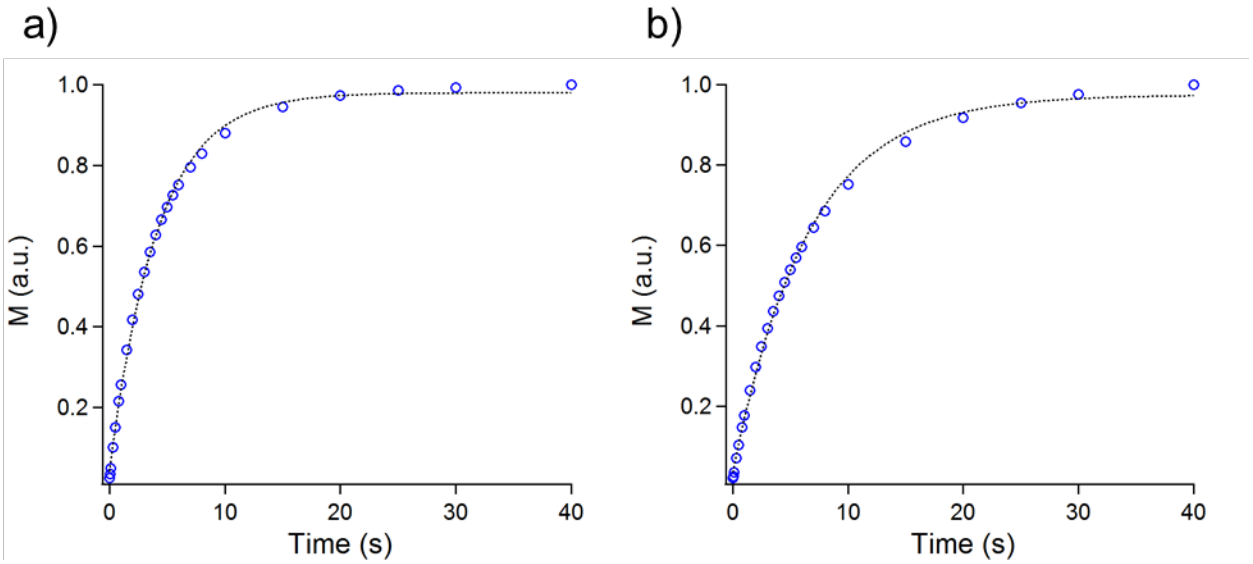

Figure S47. Fitting of saturation recovery data for **1** at a) 200 and b) 175 K

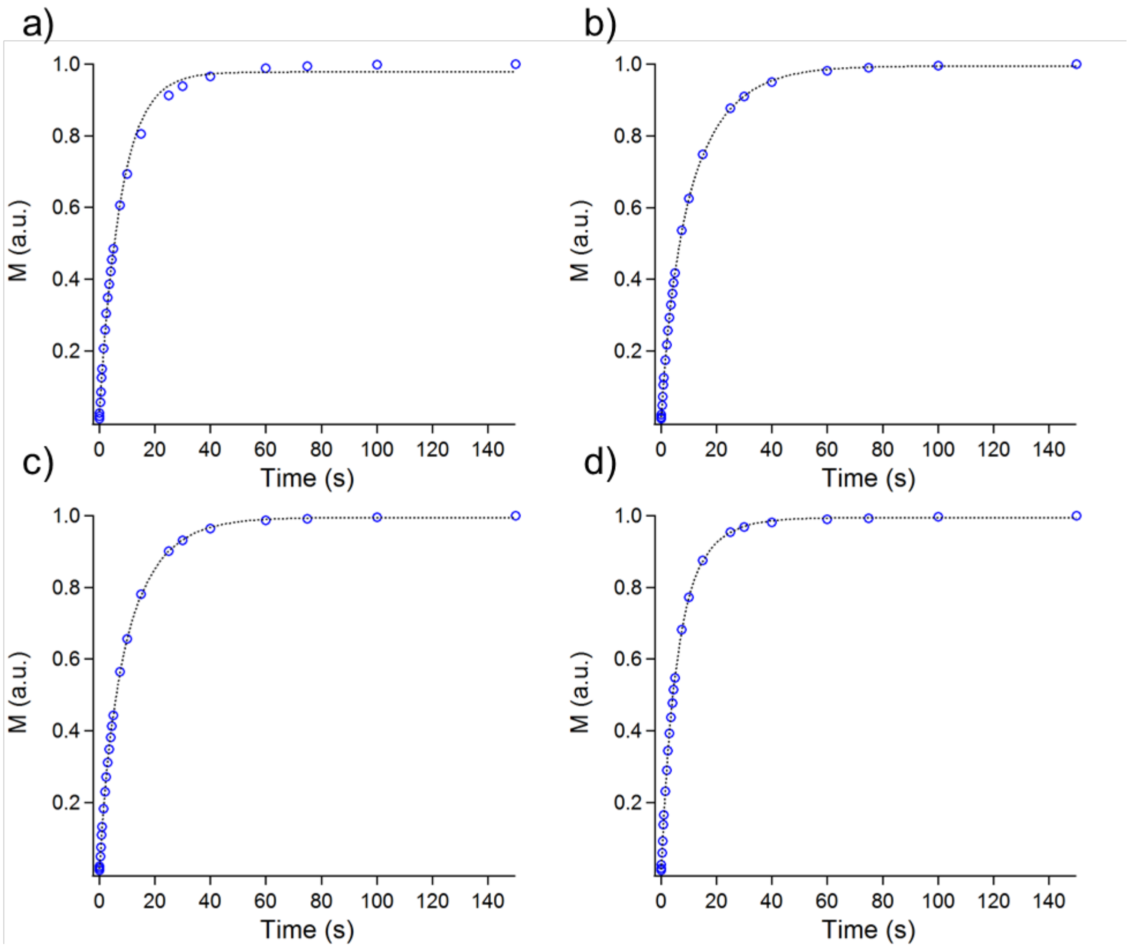

Figure S48. Fitting of saturation recovery data for **2** at a) 300, b) 275, c) 250 and d) 225 K

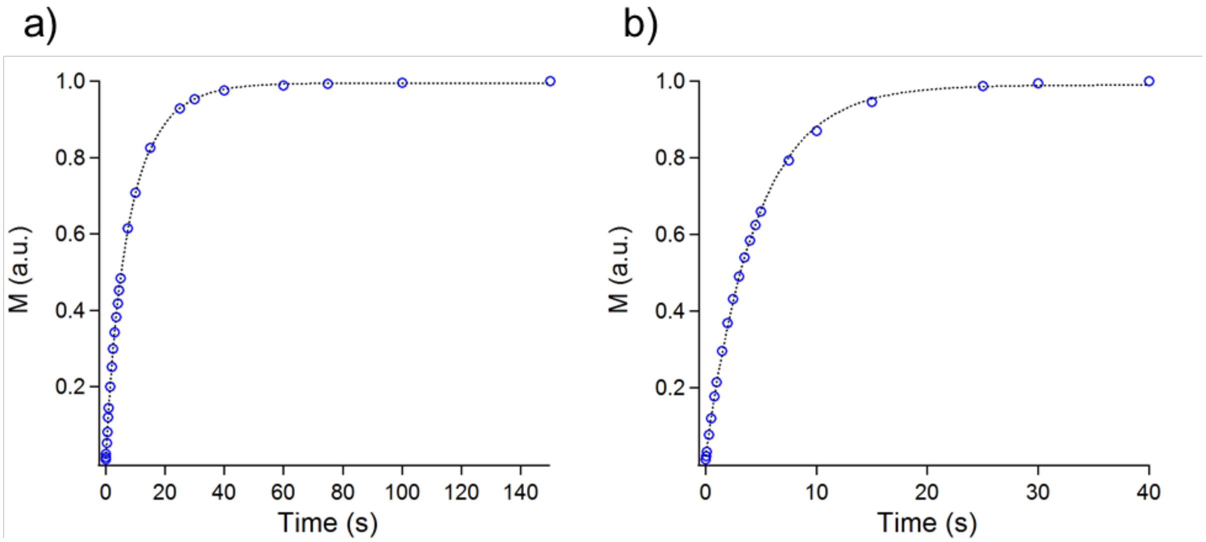

Figure S49. Fitting of saturation recovery data for **2** at a) 200 and b) 175 K

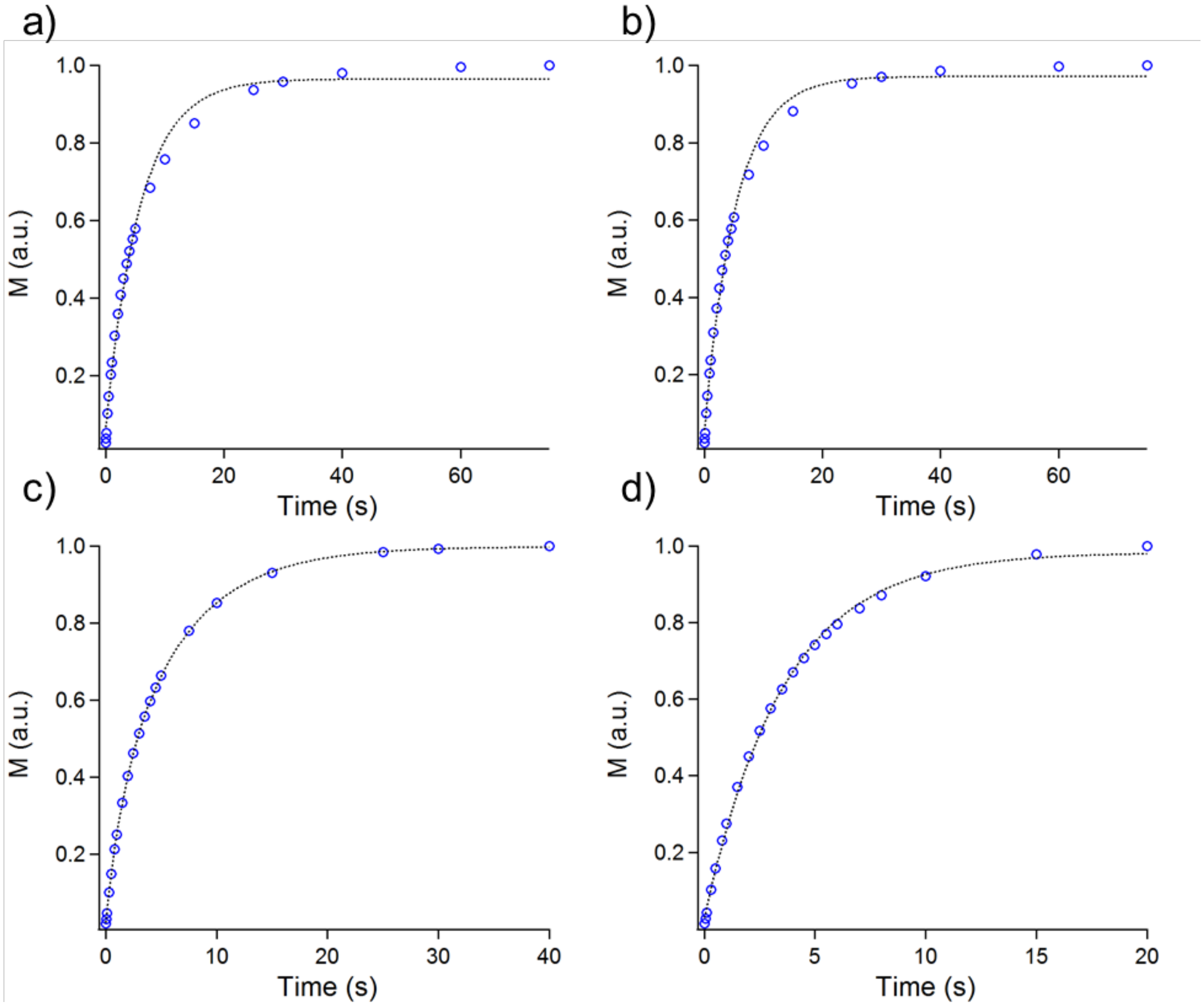

Figure S50. Fitting of saturation recovery data for **3I** at a) 300, b) 275, c) 250 and d) 225 K

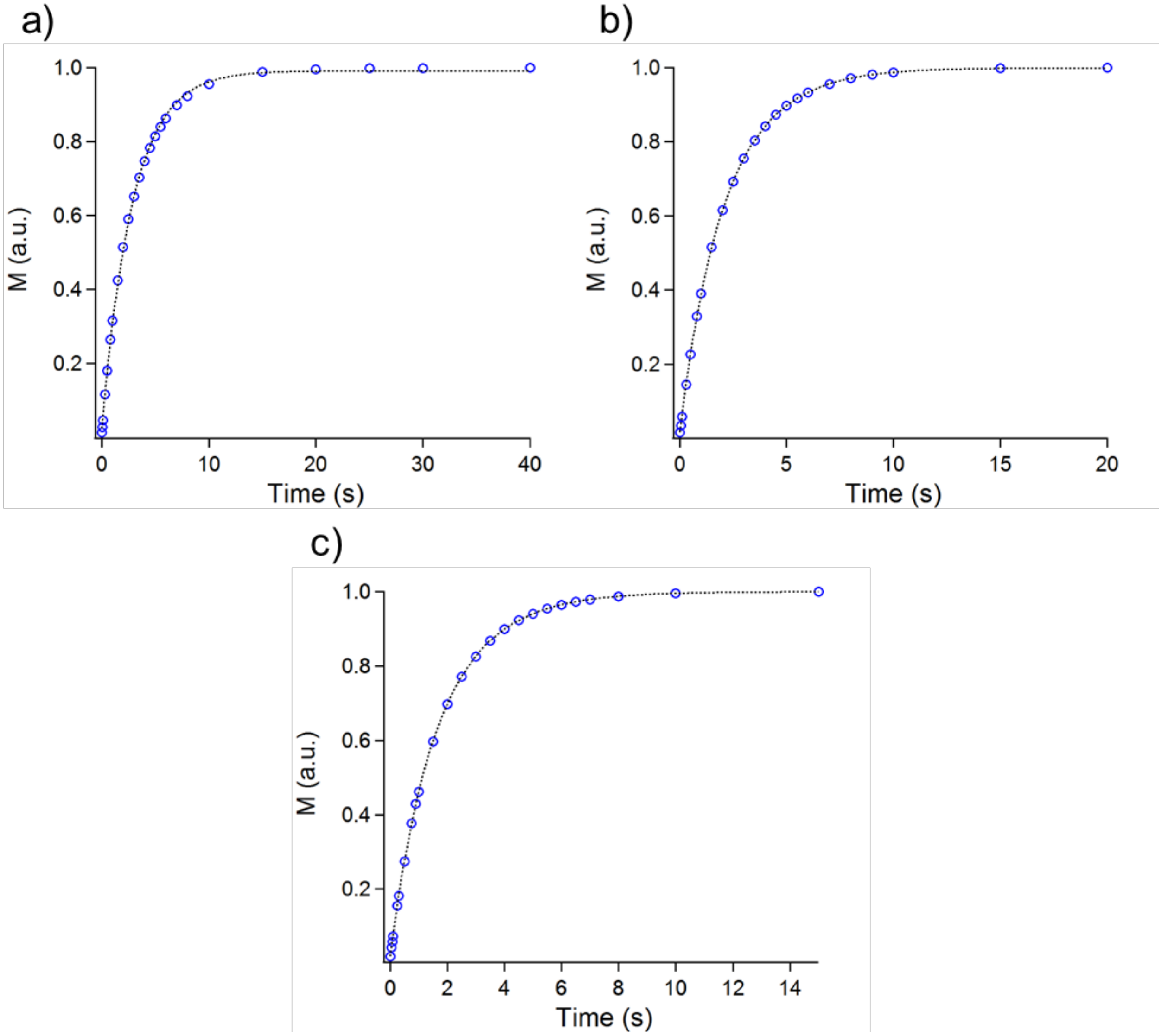

Figure S51. Fitting of saturation recovery data for **3I** at a) 200, b) 175 and c) 150 K

Voids and Hirshfeld surface analysis

Voids were generated with tool integrated in Mercury 4.3.1, according with description in figures. Hirshfeld and shape index surfaces were calculated using TONTO,[14] integrated in the software CrystalExplorer 17.[15]

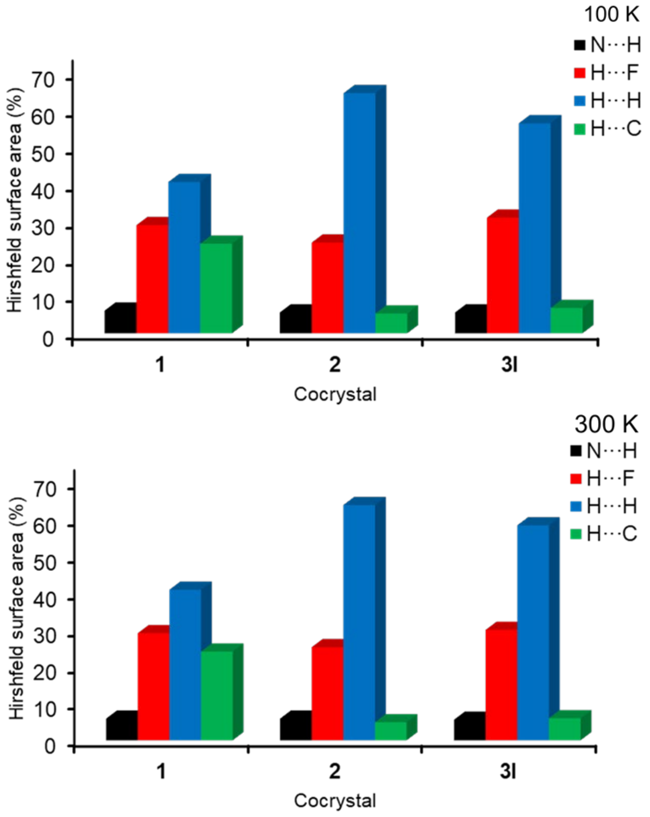

Figure S52. Contributions of intermolecular interactions onto the DABCO Hirshfeld Surface mapped for rotors herein reported.

Table S14. Numerical values for main intermolecular contributions on DABCO surface mapped

Cocrystal	**1**		**2**		**3I**	
Temperature	100 K	300 K	100 K	300 K	100 K	300 K
N···H	6.1%	5.9%	5.6%	5.9%	5.6%	5.6%
H···F	29.1%	29.1%	24.4%	25.3%	31.1%	30.0%
H···H	40.7%	40.9%	64.6%	63.9%	56.5%	58.4%
H···C	24.1%	24.1%	5.3%	4.9%	6.8%	6.0%

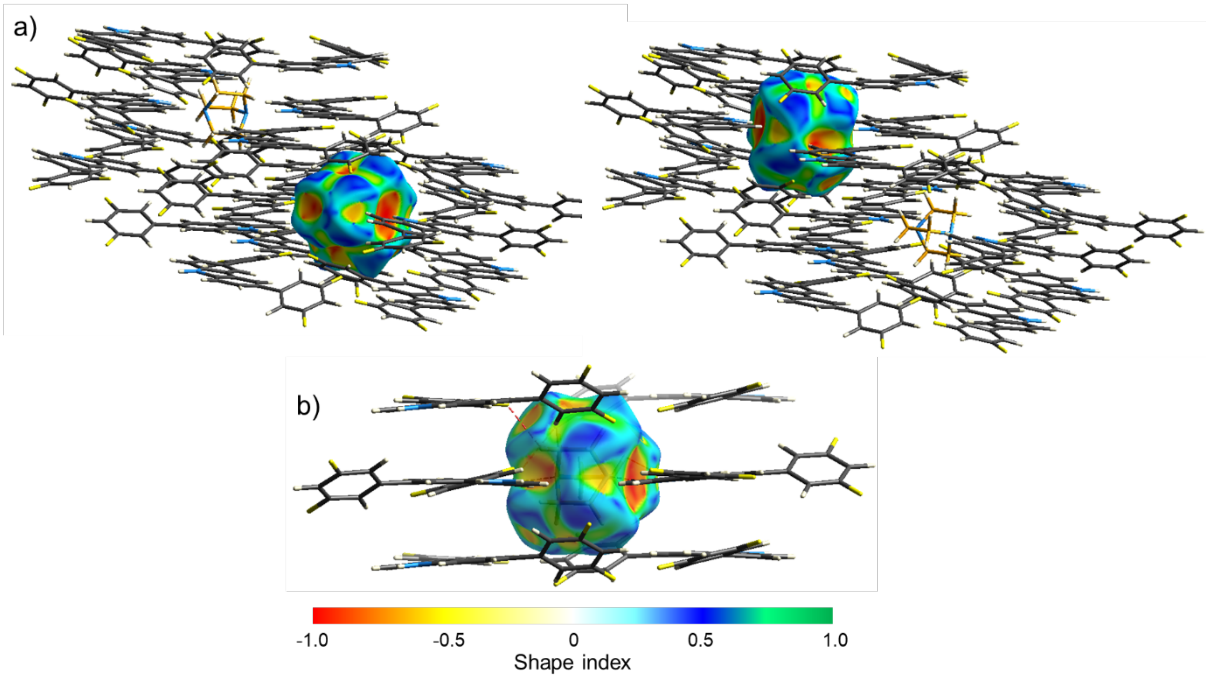

Figure S53. Shape index surfaces for cocrystal **1**, mapped from -1.0 to 1.0 at a) 100 K (both symmetrically inequivalent DABCO mapped), with mean value of 0.2746, accounting both surfaces and b) 300 K, 0.2781.

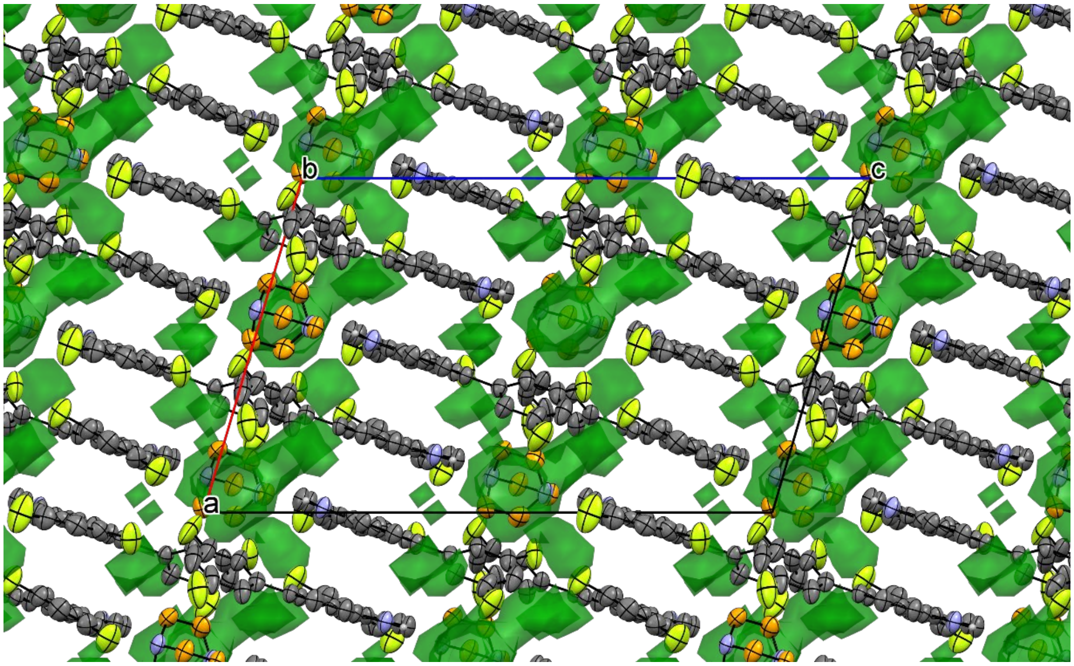

Figure S54. Voids in lattice of rotor **1** (300 K) with 0.6 Å probe radius and 0.7 Å grid spacing. The void volume accounts for 5.3%, 229.4 Å^3. Ellipsoids plotted at 50% probability level. Hydrogen atoms omitted for better visualization.

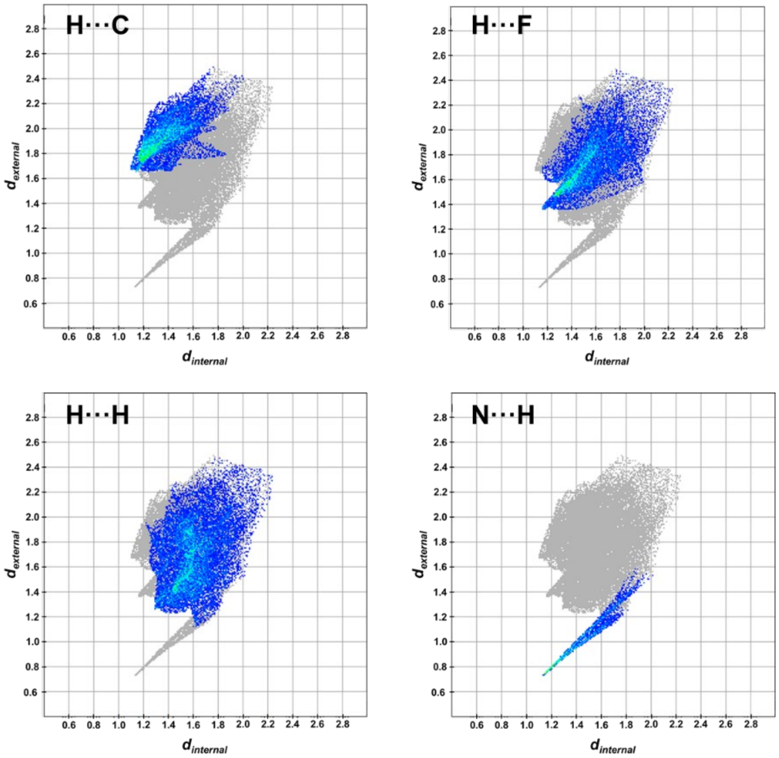

Figure S55. Hirshfeld fingerplots for DABCO in cocrystal **1-HT**. Blue colored surfaces showed account for contributions of 24.1 (up, left), 29.1 (up, right), 40.9 (down, left) and 5.9% (down, right) of the total mapped surface.

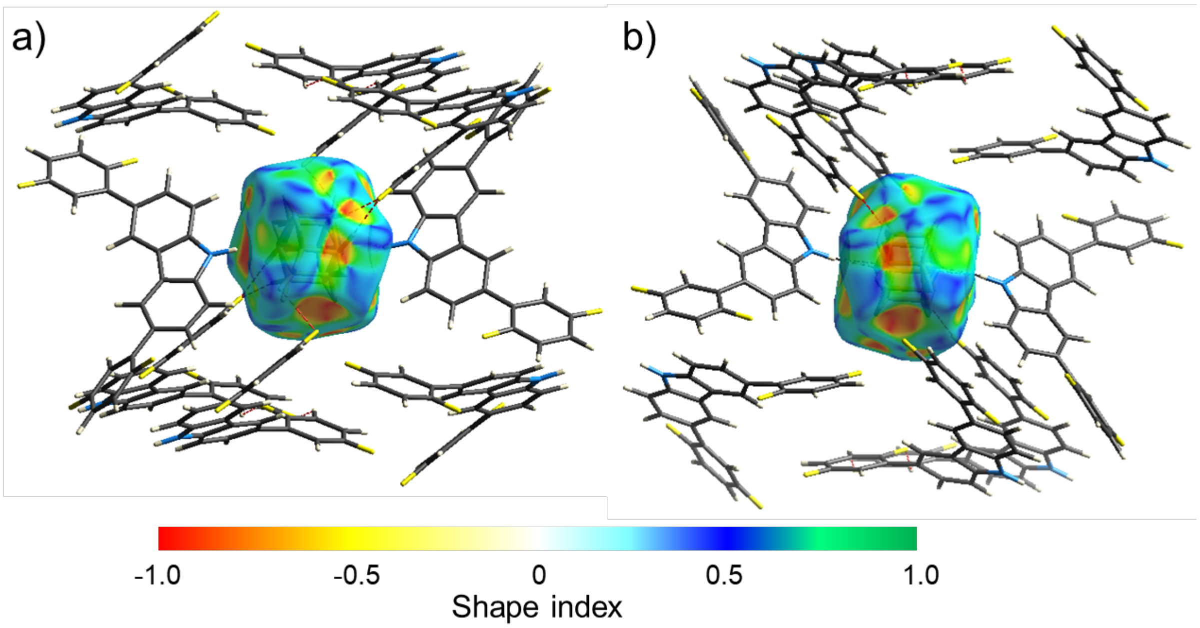

Figure S56. Shape index surfaces for cocrystal **2**, mapped from -1.0 to 1.0 at a) 100 K, with mean values of 0.2310, and b) 300 K, 0.2228.

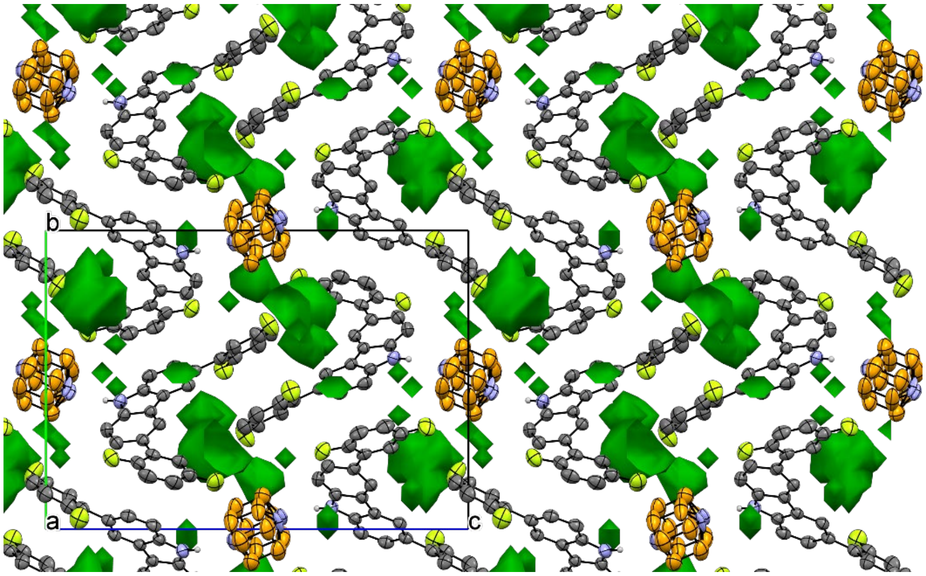

Figure S57. Voids in lattice of rotor **2** (300 K) with 0.6 Å probe radius and 0.7 Å grid spacing. The void volume is 3.3%, 71.13 Å^3. Ellipsoids plotted at 50% probability level. Hydrogen atoms omitted for better visualization.

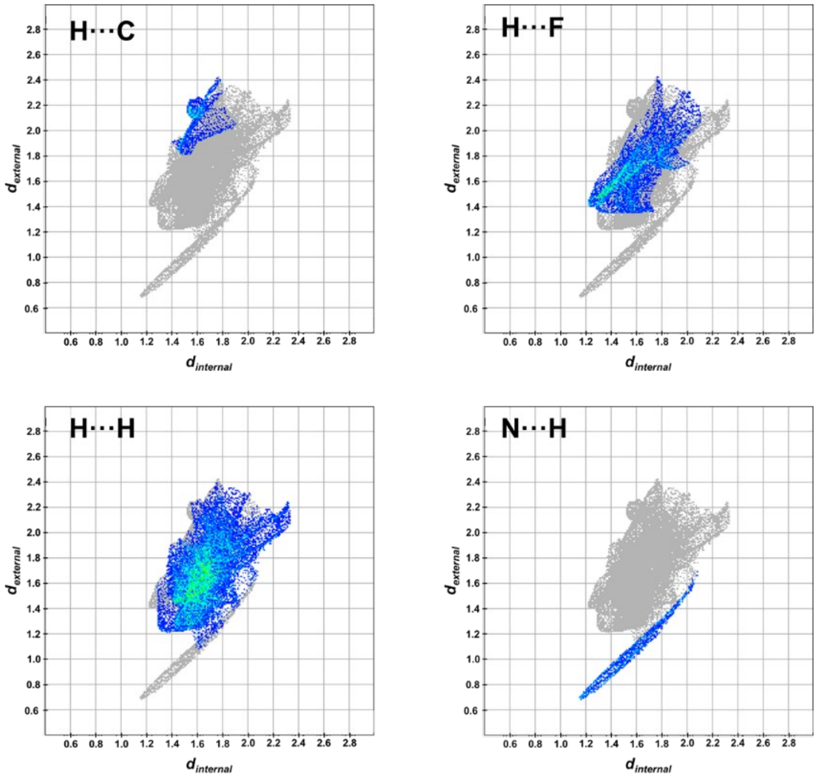

Figure S58. Hirshfeld fingerplots for DABCO in cocrystal **2** at 300 K. Blue colored surfaces showed account for contributions of 4.9 (up, left), 25.3 (up, right), 63.9 (down, left) and 5.9% (down, right) of the total mapped surface.

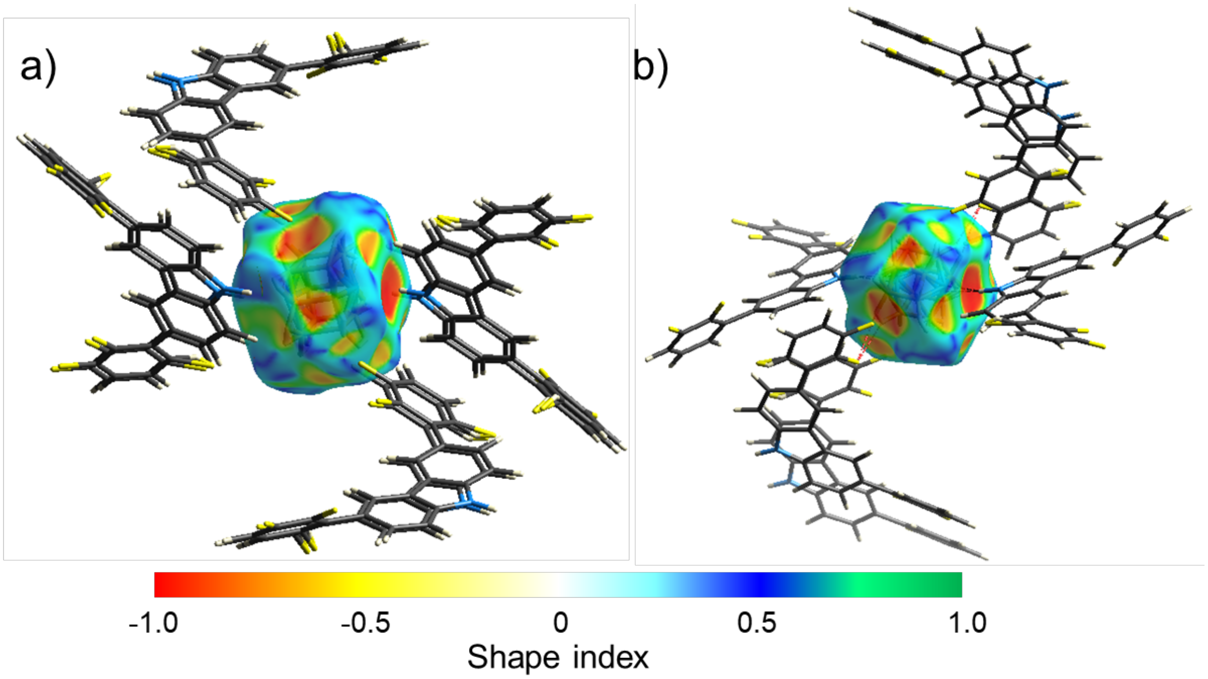

Figure S59. Shape index surfaces for cocrystal **3I**, mapped from -1.0 to 1.0 at a) 100 K, with mean values of 0.2114, and b) 300 K, 0.2172.

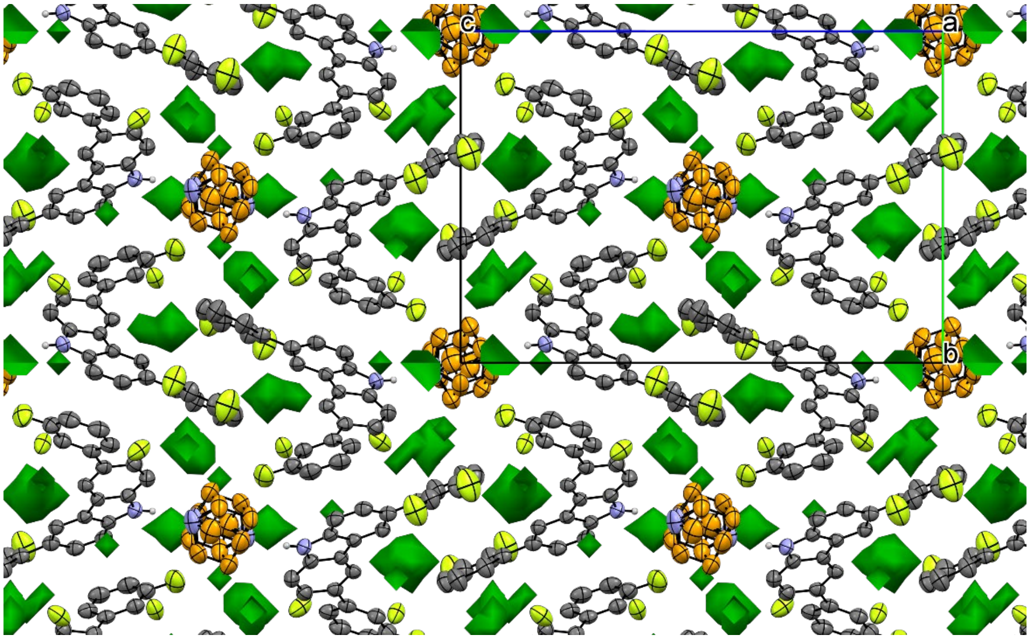

Figure S60. Voids in lattice of rotor **3I** with 0.6 Å probe radius and 0.7 Å grid spacing. The void volume is 2.1%, 44.0 Å^3. Ellipsoids plotted at 50% probability level. Hydrogen atoms omitted for better visualization.

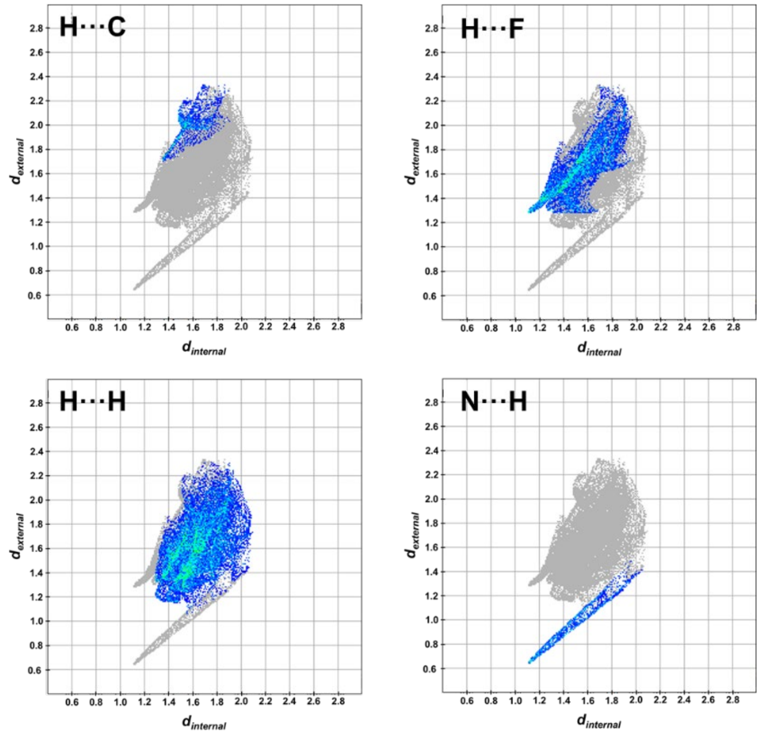

Figure S61. Hirshfeld fingerplots for DABCO in cocrystal **3I** at 300 K. Blue colored surfaces showed account for contributions of 6.0 (up, left), 30.0 (up, right), 58.4 (down, left) and 5.6% (down, right) of the total mapped surface.

References

[S1] L. Catalano, S. Perez-Estrada, G. Terraneo, T. Pilati, G. Resnati, P. Metrangolo and M. A. Garcia-Garibay, *J Am. Chem. Soc.*, 2015, **137**, 49, 15386-15389.

[S2] APEX2 Version 2008.3-0/2.2-0, Bruker AXS, Inc., Madison, WI, 2007.

[S3] Bruker. (2006b). SAINT, Version 8.38 (Bruker AXS Inc.).

[S4] G. M. Sheldrick, *Acta Cryst. A.*, 2008, **64**, 112–122.

[S5] C. F. Macrae, I. Sovago, S. J. Cottrell, P. T. A. Galek, P. McCabe, E. Pidcock, M. Platings, G. P. Shields, J. S. Stevens, M. Towler and P. A. Wood, *J. Appl. Cryst.*, 2020, **53**, 226-235.

[S6] Collection of the crystal at this temperature was carried out, however, high twinning resulted in several A-Type alerts during the CHECKCIF validation. Because of this we only report the refined cell parameters.

[S7] The diffraction pattern showed twinning and this was solved using the Cell_now tool, from which two orientation matrices were determined. The relationship between these components was determined to be 180 degrees about reciprocal axis 1 0 0. The data were integrated using the two matrices in SAINT. TWINABS was used to produce a merged file, for structure solution, initial refinement and final structure refinement. The resulting file contained the merged reflections first component and those that overlapped with this component, which were split into 2 reflection. TWINABS indicated the twin faction to be 73:27.

[S8] G. Kresse and J. Furthmüller, *Phys. Rev. B Condens. Matter*, 1996, **54**, 11169–11186.

[S9] G. Kresse and J. Furthmüller, *Comput. Mater.*, 1996, **6**, 15–50.

[S10] G. Kresse and D. Joubert, *Phys. Rev. B*, 1999, **59**, 1758–1775.

[S11] J.P. Perdew and K. Burke, M. Ernzerhof, Phys. Rev. Lett., 1996, **77**, 3865–3868.

[S12] S. Grimme, J. Antony, S. Ehrlich and H. Krieg, *J. Chem. Phys.*, 2010, **132**, 154104.

[S13] (a) J G. Mills, H. Jonsson and G. K. Schenter, *Surface Science*, 1995, **324**, 305; (b)H. Jonsson, G. Mills and K. W. Jacobsen, `Nudged Elastic Band Method for Finding Minimum Energy Paths of Transitions', in `Classical and Quantum Dynamics in Condensed Phase Simulations', ed. B. J. Berne, G. Ciccotti and D. F. Coker (World Scientific, 1998)

[S14] D. Jayatilaka, D. J. Grimwood, A. Lee, A. Lemay, A. J. Russel, C. Taylor, S. K. Wolff, P. Cassam-Chenai and A. Whitton, (2005). *TONTO – A System for Computational Chemistry.* Available at: http://hirshfeldsurface.net/

[S15] Turner, M. J., McKinnon, J. J., Wolff, S. K., Grimwood, D. J., Spackman, P. R., Jayatilaka, D. & Spackman, M. A. (2017). CrystalExplorer 17.5. The University of Western Australia.